

# Astrocyte aquaporin mediates a tonic water efflux maintaining brain homeostasis


Reviewed Preprint

v2 • October 15, 2024

Revised by authors


Reviewed Preprint

v1 • April 11, 2024

Cuong Pham, Yuji Komaki, Anna Deàs-Just, Benjamin Le Gac, Christine Mouffle, Clara Franco, Agnès Chaperon, Vincent Vialou, Tomokazu Tsurugizawa , Bruno Cauli , Dongdong Li 

Sorbonne Université, Institute of Biology Paris Seine, Neuroscience Paris Seine, CNRS UMR8246, INSERM U1130, Paris, France • Central Institute for Experimental Animals, Kawasaki, Japan • Human Informatics and Interaction Research Institute, National Institute of Advanced Industrial Science and Technology (AIST), Tsukuba, Japan • Faculty of Engineering, University of Tsukuba, Tsukuba, Japan

 [https://en.wikipedia.org/wiki/Open\\_access](https://en.wikipedia.org/wiki/Open_access)

 Copyright information

## Abstract

Brain water homeostasis not only provides a physical protection, but also determines the diffusion of chemical molecules key for information processing and metabolic stability. As a major type of glia in brain parenchyma, astrocytes are the dominant cell type expressing aquaporin water channel. How astrocyte aquaporin contributes to brain water homeostasis in basal physiology remains to be understood. We report that astrocyte aquaporin 4 (AQP4) mediates a tonic water efflux in basal conditions. Acute inhibition of astrocyte AQP4 leads to intracellular water accumulation as optically resolved by fluorescence-translated imaging in acute brain slices, and *in vivo* by fiber photometry in mobile mice. We then show that aquaporin-mediated constant water efflux maintains astrocyte volume and osmotic equilibrium, astrocyte and neuron  $\text{Ca}^{2+}$  signaling, and extracellular space remodeling during optogenetically induced cortical spreading depression. Using diffusion-weighted magnetic resonance imaging (DW-MRI), we observed that *in vivo* inhibition of AQP4 water efflux heterogeneously disturbs brain water homeostasis in a region-dependent manner. Our data suggest that astrocyte aquaporin, though bidirectional in nature, mediates a tonic water outflow to sustain cellular and environmental equilibrium in brain parenchyma.

## Significance statement

Our brain is immersed, thus protected, in a water environment. It ensures intra- and extracellular molecular diffusion, which is vital for brain function and health. Brain water homeostasis is maintained by dynamic water transport between different cell types. Astrocytes are a main type of glial cell widely distributed in brain parenchyma, expressing the bidirectional aquaporin water channel. Here we show that in basal conditions, aquaporin channel mediates a tonic water efflux from astrocytes. This mechanism maintains astrocyte volume stability, activity-gated brain parenchyma remodeling and brain water homeostasis. Our finding sheds light on how astrocytes regulate water states in the brain, and will help to understand brain allostasis in specific life contexts.

### eLife Assessment

In this work, the authors propose that astrocytic aquaporin 4 (AQP4) is the main pathway for tonic water efflux, without which astrocytes undergo cell swelling. These findings are **important**, because they shed light on key molecular mechanisms implicated with the regulation of brain water homeostasis. The authors use a broad set of experimental tools (e.g., acute brain slices, in vivo recording, and diffusion-weighted MRI) but the evidence remains **incomplete** without ruling out non-specific effects of TGN-020, and without evidence that changes in sulforhodamine B fluorescence can be used as reliable readouts of cell volume dynamics.

<https://doi.org/10.7554/eLife.95873.2.sa3>

## Introduction

Every aspect of brain function relies on the delicately maintained water environment. It supports brain structural stability and molecular diffusion, laying the ground for information processing, metabolite shuttling and adaptation to living environments (Kimelberg, 2004). Water is the fundamental constituent of the cerebrospinal fluid infiltrating into the central nervous system and the interstitial fluid distributed in brain parenchyma (Agnati et al., 2017; Brinker et al., 2014). Brain fluid transport is suggested to support the diffusion of energetic fuels like glucose and lactate to warrant the metabolic circumstances in the parenchyma, and is also implicated in the clearance of waste molecules from the brain as described in the glymphatic system (Abbott et al., 2018; Iliff et al., 2013; Iliff et al., 2012; Mestre et al., 2018a; Rasmussen et al., 2022). In addition, the restricted mobility of water molecules diffusion within intra- and extracellular space reflects the brain microstructure. The diffusion-weighted magnetic resonance imaging (DW-MRI) detects the mobility of water proton for structural and functional neuroimaging (Le Bihan et al., 2006; Tsurugizawa et al., 2013), being adopted for clinical diagnostics in neurological diseases such as ischemia, brain tumor and edema (Gaddamanugu et al., 2022; Le Bihan and Iima, 2015) and recently leveraged for assessing brain glymphatic system (Giannetto et al., 2024; Gomolka et al., 2023).

Water equilibrium in the brain is maintained by dynamic transport between different cell entities. Aquaporin is a family of transmembrane channels facilitating bidirectional water flow, with aquaporin 4 (AQP4) being the main subtype expressed in the central nervous system. In the brain, AQP4 is expressed in astrocytes (Papadopoulos and Verkman, 2013; Xiao et al., 2023) that are a major type of glial cell in the parenchyma (Barres, 2008). This feature enables astrocytes to well balance osmotic oscillations imposed by the transmembrane transport of ions, metabolites, and signaling molecules, all mediated by water. AQP4 has been proposed to maintain the circulation of cerebrospinal fluid (CSF), underlying the clearance efficacy of glymphatic system (Hablitz et al., 2020; Kress et al., 2014; Mestre et al., 2018a; Smith et al., 2017). Dysregulation in astrocyte aquaporin water transport is implicated in pathological scenarios such as cerebral edema and neuroinflammation (Verkman et al., 2011). Valuable insights have been obtained on the function of astrocyte aquaporin in specific physiopathological conditions including osmotically evoked volume responses, ischemia and neurodegenerative diseases (Verkman et al., 2017). Meanwhile, how astrocyte aquaporin contributes to brain water homeostasis in basal physiology has remained elusive. A better understanding will aid to discern astrocytic regulation of cerebral water states, thereby the potential maladaptations in neurological disorders.

Here, combining *in vivo* chemical targeting, optical and MRI imaging of water dynamics, we report that AQP4 sustains a tonic water efflux from brain astrocytes. This mechanism was found to be critical in maintaining astrocyte volume and signaling stability, as well as the extracellular space remodeling in mouse cortex during optogenetically induced cortical spreading depression. Using DW-MRI, we observed that acute inhibition of astrocyte water efflux *in vivo* heterogeneously alters water diffusion across brain regions. Our finding suggests that aquaporin acts as a water export route in astrocytes in physiological conditions, contributing to maintain cellular and parenchymal water equilibrium.

## Results

### Astrocyte aquaporin mediates a tonic water efflux

To optically follow astrocyte water transport *in situ*, we performed real-time imaging of sulforhodamine B (SRB)-labeled astrocytes, whose fluorescence changes reflect real-time volume oscillation due to transmembrane water flux. We chemically labeled mouse brain astrocytes *in vivo* with a highly water-diffusible and astrocyte-specific red fluorescent dye, sulforhodamine B (SRB) (**Figure 1A**, *top*) (Appaix et al., 2012; Pham et al., 2020). About one hour after its intraperitoneal injection, astrocytic SRB labeling was widely distributed in the mouse cortex, as seen in living acute brain slices (**Fig. 1A**, *middle*) and validated by colocalization with EGFP-identified astrocytes in slices taken from GFAP-EGFP transgenic mice (**Fig. 1A**, *bottom*). Net water transport across the astrocyte membrane alters cytoplasmic SRB concentration and cellular volume, which can thus be followed by changes in fluorescence intensity when imaged in a fixed field of view. To validate this fluorescence intensity-translated (FIT) imaging of astrocyte water transport, we employed wide-field fluorescence microscopy for single-plane time-lapse imaging in acute brain slices in the primary somatosensory (S1) cortex. This approach allowed us to collect fluorescence from both the focal plane and along the axial extension, thereby imprinting volumetric fluorescence into the single image plane. Indeed, water influx induced by the application of hypoosmotic solution over different periods decreased astrocyte SRB fluorescence, concomitantly reflecting the cell swelling (**Fig. 1B**, *top*); whereas water export and astrocyte shrinking upon hyperosmotic manipulation increased astrocyte fluorescence (**Fig. 1B**, *bottom*). Hence, by following the fluorescence change of SRB-labeled astrocytes, the FIT imaging strategy allows to monitor the real-time changes in astrocyte water transport and volume change.

In basal conditions, flat fluorescence time course was recorded in brain slices suggesting equilibrated water transport across the astrocyte membrane (**Fig. 1B**) and volume homeostasis in the brain parenchyma. To inspect a tonic role of aquaporin in astrocyte water transport, we sought to acutely block astrocytic aquaporin channel, aquaporin 4 (AQP4). We used the synthetic compound 2-(nicotinamido)-1,3,4-thiadiazole (TGN-020) that is derived from the condensation of nicotinamide and thiadiazole derivatives (Burnett et al., 2015; Huber et al., 2009; Igarashi et al., 2011; Sun et al., 2022), whose specificity for AQP4 has been validated *in vitro* by ion channel heterologous expression system (Toft-Bertelsen et al., 2021) and *in vivo* using the AQP4 knockout (KO) mice (Harrison et al., 2020; Igarashi et al., 2013). This approach permitted the functional pinpointing of astrocyte aquaporin under physiological conditions, while avoiding the chronic compensations caused by genetic tools and mouse models that have been reported to alter brain water content, volume and extracellular architecture potentially confounding the functional readouts (Binder et al., 2004; Gomolka et al., 2023; Haj-Yasein et al., 2011; MacAulay, 2021; Yao et al., 2015).

AQP4 is a bidirectional channel providing a path of least resistance for water transfer along the osmotic gradient (Papadopoulos and Verkman, 2013). As an osmotic equilibrium is maintained in the brain parenchyma in basal state, there might not be net water transport across AQP4. However, we observed in cortical slices that while little impact was seen with vehicle (CTR) on the

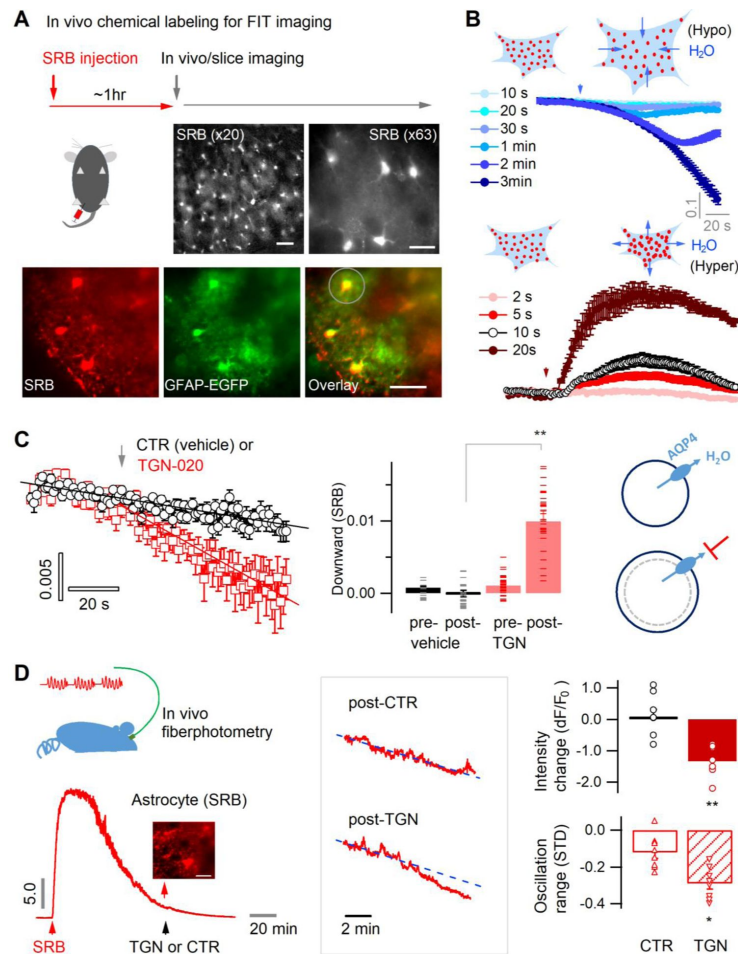


**Fig. 1.**

### Astrocyte aquaporin mediates a tonic water efflux.

**(A)** *In vivo* chemical labelling of astrocytes. Sulforhodamine B (SRB, 10 mg/ml) was intraperitoneally injected in awake mice (10  $\mu$ l/g). Monochrome images show representative astrocyte labeling in living acute brain slices from cortex under low ( $\times 20$ ; scale bar, 50  $\mu$ m) and high magnification ( $\times 63$ ; scale bar, 20  $\mu$ m) by epifluorescence. *Below*, SRB labeling was confirmed to be astrocyte-specific in acute brain slices of the astrocyte reporter line GFAP-EGFP, where light sheet imaging was used to gain optical sectioning (Materials and methods; Fig. S1). The light gray circle indicates the astrocyte regions used for fluorescence analysis. Scale bar, 50  $\mu$ m. **(B)** Optical imaging of astrocyte water transport in acute brain slices. Transmembrane water transport was triggered with hypo- and hypertonic solution, inducing water inflow and outflow that were respectively reflected by SRB fluorescence decrease (*above*) and increase (*below*; expressed as  $dF/F_0$ ). The hypo- or hypertonic solution was applied to slices over different lengths of duration displayed in colors corresponding to the time courses of SRB fluorescence ( $n = 52$  astrocytes, 4 mice). **(C)** Acutely blocking astrocyte AQP4 with TGN-020 caused intracellular water accumulation and swelling. The downward change in the SRB fluorescence was respectively calculated for the phases prior and post to vehicle or TGN application. *Left*, while no effect was seen under CTR condition (vehicle only,  $n = 23$  astrocytes, 3 mice), TGN-020 (20  $\mu$ M) significantly decreased astrocyte SRB fluorescence ( $n = 30$ , 6 mice). Imaging was performed in acute brain slices of layer II/III S1 cortex. *Middle*, the downward slope was compared between the periods before and after the application of TGN-020. *Right*, illustration shows astrocyte aquaporin sustaining a tonic water efflux. Its blockade causes water accumulation and cell swelling. **(D)** *In vivo* validation of the effect of TGN-020 application on astrocyte water homeostasis. *Left*, fiber photometry was used for real-time recording of SRB fluorescence of astrocyte population in S1 cortex in freely moving mice, with saline (CTR) or TGN-020 being intraperitoneally injected when SRB was trapped in astrocytes. Fiber photometry recording shows that *in vivo* SRB injection resulted in rapid entry into mouse cortex and, in about one hour, led to astrocyte labeling (inset scale bar, 50  $\mu$ m). *Middle*, example response to saline and TGN-020. The change of SRB fluorescence relative to the photobleaching tendency delineated by line fitting (dotted line) was examined. *Right*, relative to CTR, TGN administration led to a decrease in astrocyte SRB fluorescence and its oscillation range ( $n = 8$  recordings per condition, 5 mice).

tendency of fluorescence time courses of SRB-labeled astrocytes (**Fig. 1C**, *left and middle*), acute inhibition of astrocyte AQP4 by TGN-020 caused a gradual decline, suggesting a progressive intracellular water accumulation (**Fig. 1C**, *left and middle*). This observation implies that in basal condition, astrocyte aquaporin mediates a constant water efflux; its blocking causes intracellular water accumulation and swelling (**Fig. 1C**, *right*). To corroborate this observation *in vivo*, we performed fiber photometry recording in moving mice (**Fig. 1D**, *left*). An optical fiber was implanted into the mouse S1 cortex to follow fluorescence signals of local astrocyte population post the intraperitoneal injection of SRB (**Fig. 1D**, *left*). After about one hour, when astrocytes were labeled, either saline or TGN-020 was injected intraperitoneally. Although no significant effect was observed with the saline control, TGN-020 induced a decrease in astrocyte SRB fluorescence and a reduction in its oscillation range (**Fig. 1D**, *right*), mirroring an intracellular dilution of fluorescent molecules. Together, these observations suggest that acute inhibition of astrocyte aquaporin leads to intracellular water accumulation thereby cell swelling.

## Aquaporin inhibition perturbs astrocyte and neuron signaling

Astrocyte volume equilibrium not only determines brain structural stability, but also associates with dynamic cellular signals. Astrocyte swelling has been shown to alter intracellular  $\text{Ca}^{2+}$  signaling (Benfenati et al., 2011; Eilert-Olsen et al., 2019). We performed  $\text{Ca}^{2+}$  imaging in acute brain slices to confirm that acute aquaporin inhibition induces astrocyte swelling and then  $\text{Ca}^{2+}$  oscillation. The genetically encoded  $\text{Ca}^{2+}$  sensor GCaMP6f was selectively expressed in astrocytes by crossing the Glast-Cre<sup>ERT2</sup> and GCaMP6<sup>floxP</sup> mouse lines (Herrera Moro Chao et al., 2022; Pham et al., 2020) (**Fig. 2A**, *top*). Because astrocyte  $\text{Ca}^{2+}$  signals often occur in local domains, we adapted a light sheet microscope (Pham et al., 2020) for wide-field optical sectioning so as to image them with high signal-to-noise ratio (Fig. S1). We first confirmed that water accumulation, therefore astrocyte swelling, induced by hypotonic solution enhanced the intracellular  $\text{Ca}^{2+}$  signal (**Fig. 2A**). Then we followed astrocyte  $\text{Ca}^{2+}$  in isotonic control condition while blocking astrocyte AQP4 with TGN-020, and observed that  $\text{Ca}^{2+}$  signaling was augmented following the acute aquaporin inhibition (**Fig. 2B**). The spontaneous  $\text{Ca}^{2+}$  signals in perivascular astrocyte end-feet, which wrapped the blood vessels displaying as tube-like structures, showed relatively higher sensitivity to the acute application of TGN-020, consistent with the enrichment of AQP4 in the end feet (Fig. S2). This result confirms that inhibiting astrocyte tonic water efflux would have led to intracellular water accumulation and swelling, thus altering the astrocytic  $\text{Ca}^{2+}$  signaling. In addition, astrocyte swelling has been reported to induce the release of neuroactive molecules such as glutamate thereby influencing nearby neuron activity (Fiacco et al., 2007; Yang et al., 2019). Disrupting AQP4 tonic water outflow may not only cause astrocyte swelling but also influence the activity of neighboring neurons. We then imaged  $\text{Ca}^{2+}$  signals as a surrogate for neuronal activity in cortical somatostatin (SST) interneurons which exhibit high excitability (Karagiannis et al., 2021) and express both ionotropic and metabotropic glutamate receptors (Cauli et al., 2000), rendering them ideal to sense astrocyte-released signaling molecules. We expressed GCaMP6f in SST interneurons by crossing homozygous SST-Cre (Taniguchi et al., 2011) and homozygous GCaMP6<sup>floxP</sup> mice. TGN-020 inhibition of astrocyte AQP4 led to a global  $\text{Ca}^{2+}$  elevation in SST interneuron populations (**Fig. 2C**). These observations suggest that astrocyte aquaporin mediates a tonic water efflux, contributing to maintain both the volume and signaling homeostasis.

## Aquaporin water efflux regulates astrocyte volume response

We then examined the role of aquaporin water efflux in astrocyte volume response to osmotic changes. The AQP4 blocker TGN-020 or equimolar vehicle was applied throughout the recording, namely being continuously present before and after osmotic challenges. We first followed the evoked water efflux and shrinking induced by hypertonic solution. As astrocyte AQP4 supports preferentially water efflux, its inhibition would attenuate hypertonicity-imposed water extrusion (**Fig. 3A**). Supporting this, application of TGN-020 slowed down the hypertonicity-induced water

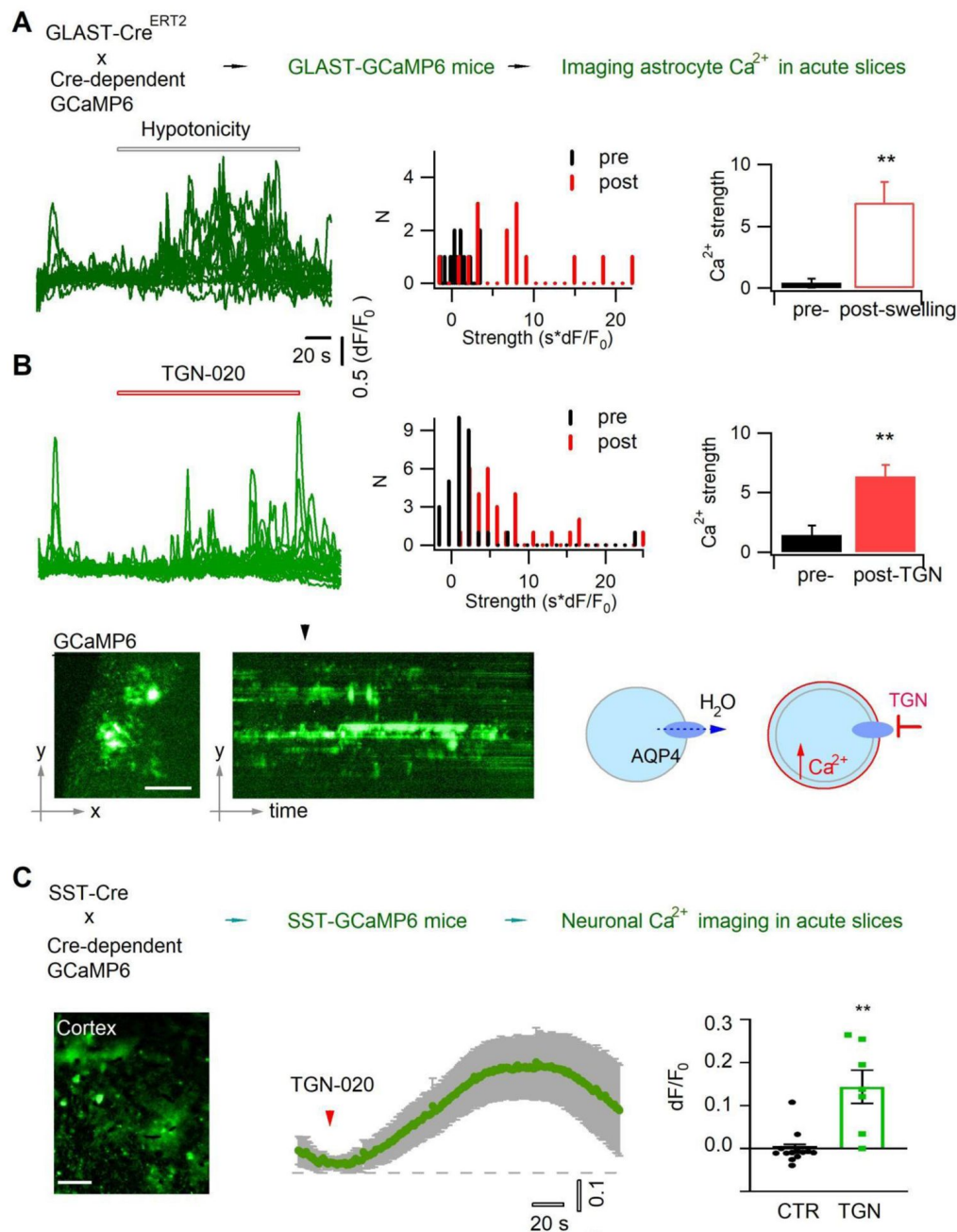


**Fig. 2.**

### Acutely blocking astrocyte aquaporin induces swelling-associated Ca<sup>2+</sup> oscillation.

(A) *In vivo* expression in astrocytes of the genetically encoded fluorescent Ca<sup>2+</sup> indicator GCaMP6 for imaging astrocyte Ca<sup>2+</sup> in acute brain slices. Angular light sheet microscopy (Fig. S1) was used to capture transient Ca<sup>2+</sup> signals of local regions. As a positive control, astrocyte swelling was induced by hypotonic solution (100 mOsm) that caused Ca<sup>2+</sup> changes from their homeostatic level. *Left*, representative time courses of swelling-induced Ca<sup>2+</sup> changes in detected response regions; *middle to left*, the histogram distribution and bar representation showing the signal strengths that were derived from the temporal integral of individual Ca<sup>2+</sup> time courses normalized per minute, before and after cell swelling ( $n = 15$  ROIs, from three mice). (B) Astrocyte Ca<sup>2+</sup> oscillation caused by acute aquaporin blocking with TGN-020 (20  $\mu$ M,  $n = 31$  ROIs, from five mice), due to the inhibition of the tonic water efflux that led to astrocyte swelling as illustrated. Time scale and Ca<sup>2+</sup> rise scale ( $dF/F_0$ ) are the same as in A. Scale bar, 50  $\mu$ m. (C) Intercellular effect on SST interneurons of blocking astrocyte aquaporin water efflux. TGN-020 (20  $\mu$ M) or the equal molar vehicle (CTR) was bath applied to acute cortical slices of SST-GCaMP6 mice ( $n = 7$ -12 regional measurements from four mice). Scale bar, 50  $\mu$ m.

efflux and shrinking, reflected by the longer time to peak in the SRB fluorescence time course as compared to control (**Fig. 3B**, left), though the delay in the initial onset was not significantly prolonged (**Fig. 3B**, right). The maximal increase in astrocyte SRB fluorescence was lower in the presence of TGN-020, suggesting that AQP4 blocking reduced the overall amount of water efflux (**Fig. 3B**, right).

We next evoked water influx, thereby astrocyte swelling, by hypotonic solution in the presence or absence of TGN-020 (**Fig. 3C**). In contrast to the effects on hypertonicity-evoked water efflux, AQP4 acute inhibition was observed to accelerate both the initial water accumulation and the swelling rate in astrocytes, reflected by their earlier onset in SRB fluorescence decrease and faster reaching to the plateau value relative to the control condition (**Fig. 3D**). This observation cross-validates the role of astrocyte aquaporin in supporting water efflux, whereby its blockade facilitates the initial accumulation of the evoked water influx (**Fig. 3C**). In contrast, the late-stage maximum decrease in astrocyte SRB fluorescence was observed to be reduced in the presence of TGN-020 (**Fig. 3D**, right), reflecting a reduction in the total amount of water accumulation and swelling. As TGN-020 was present prior to hypotonic challenge, it would have slightly swelled astrocytes due to the blockade of tonic water efflux, thereby constraining the range of further swelling induced by subsequent hypotonicity. In addition, while astrocyte AQP4 sustains a water outflow in basal physiology, in conditions when transmembrane water gradient is altered as occurred in hypotonic solutions, the net water flow through AQP4 should be finally dictated by the osmotic gradient due to its bidirectional nature. Therefore, along the imposed hypotonicity, AQP4 started to instruct a water influx; its constant blocking by TGN-020 would have reduced the total amount of water influx thereby the maximal extent of swelling.

Astrocytes are widely distributed throughout the brain parenchyma, orchestrating water transport and volume homeostasis (Ochoa-de la Paz and Guliás-Canizo, 2022). Water outflow via astrocyte AQP4 may play a role in the structural remodeling of parenchyma at the global level. We then induced general cell swelling and changes in extracellular spaces by triggering cortical spreading depression (CSD), a widespread depolarization implicated in brain physiopathology (Chung et al., 2019; Holthoff and Witte, 1996; Zhao et al., 2019). To be orthogonal to the pharmacological control of astrocyte aquaporin, the CSD depolarization wave was initiated by optogenetically stimulating ChR2-expressing glutamatergic pyramidal cells in the cortical slices of *Emx1-Cre::Ai32ChR2* mice (Gorski et al., 2002; Madisen et al., 2012), termed Opto-CSD. As cell swelling increases the transmittance of infrared light, we imaged Opto-CSD by the intrinsic optical signal (IOS) derived from infrared illumination (Holthoff and Witte, 1996; MacVicar and Hochman, 1991), which was spectrally distinct from ChR2 photoactivation (detailed in Methods). The IOS displayed transient increase across cortical layers during the Opto-CSD (**Fig. 4A-C**), exhibiting propagating kinetics characteristic of spreading depression (Chung et al., 2019; Holthoff and Witte, 1996). The biphasic starting of IOS coincided with a sharp response in the extracellular potential indicating the CSD initiation (Fig. S3A). IOS signal contains a first peak reflecting the rapid CSD response (**Fig. 4C, b**) followed by a prolonged phase of general cellular swelling (**Fig. 4C, c**). By combining fluorescence imaging of SRB-labelled astrocytes, whose spectrum is separated from the IOS infrared signal, we observed that astrocytes swelling (i.e., decrease in SRB fluorescence) paralleled CSD swelling (Fig. S4). Consistent with our observation on astrocyte volume response (**Fig. 3D**), when pre-incubating slices with TGN-020 to block AQP4 water outflow, the initiation of both the CSD and general swelling was accelerated while their maximum amplitude reduced (**Fig. 4D-E**; Fig. S3B). Indeed, TGN-020 also increased the speed and the duration of the swelling while prolonging the recovery time from the swelling, confirming acute inhibition of AQP4 water efflux facilitates astrocyte swelling while restrains shrinking (Fig. S5). Blocking action potentials with tetrodotoxin (TTX) only reduced the amplitude of the initial CSD response while the effect on general swelling is insignificant (**Fig. 4D-E**). We further followed the swelling of individual SRB-labelled astrocytes during Opto-CSD. In consistence with the result obtained from hypotonic challenge (**Fig. 3D**, right), the presence of TGN-020 reduced the peak amplitude of astrocyte swelling (i.e., the maximal SRB fluorescence decrease; **Fig. 4F**).

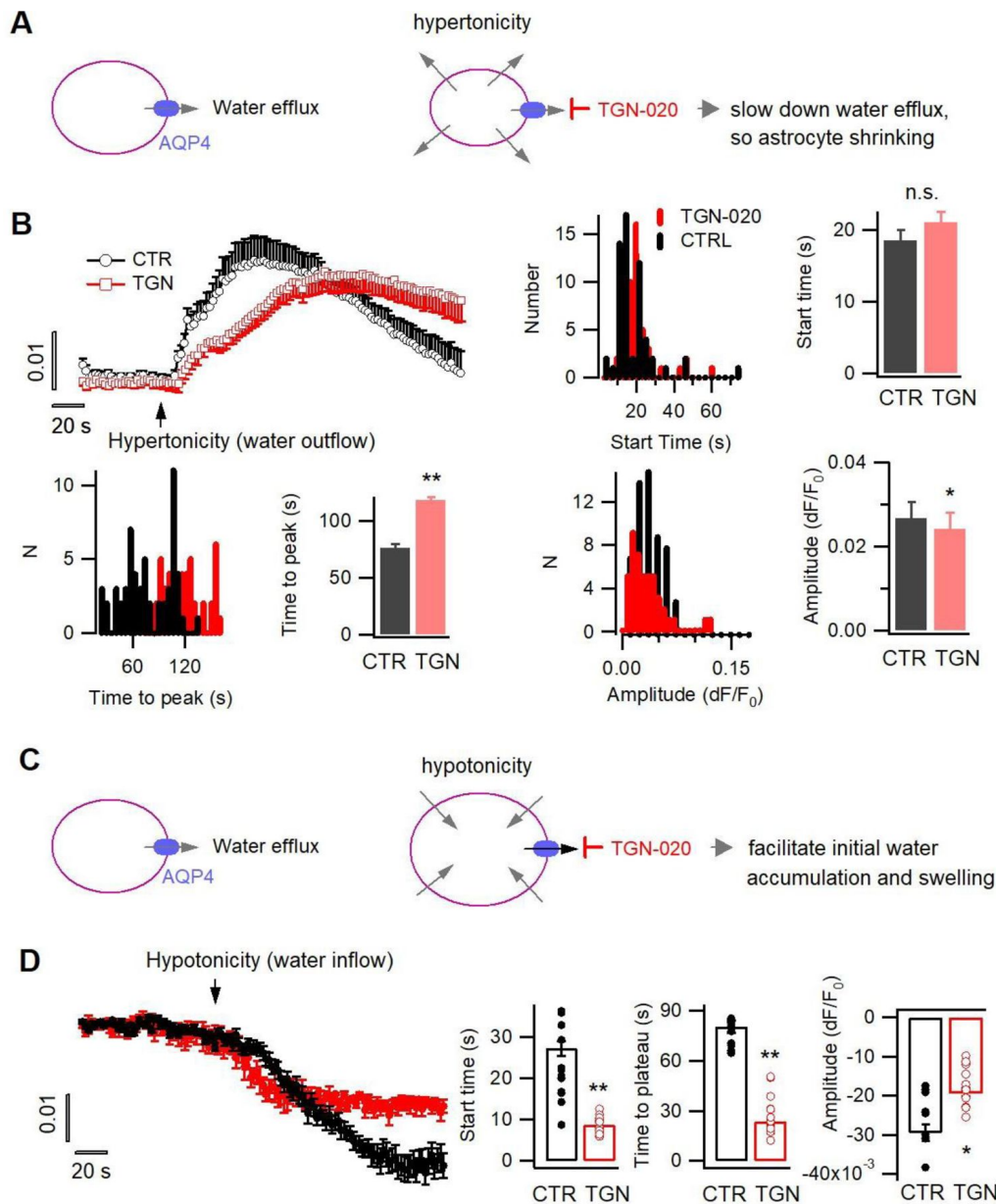


**Fig. 3.**

### Tonic water efflux via aquaporin modulates phasic transmembrane water transport and astrocyte volume response.

(A) *Left*, in basal condition astrocyte aquaporin mediates a tonic water efflux. *Right*, protocol to induce water outflow from astrocytes, therefore their shrinking, by hypertonic extracellular solution (400 mOsm) in either control condition (CTR) or in the presence of AQP4 inhibitor TGN-020 (20  $\mu$ M). (B) Time courses of astrocyte SRB fluorescence increase upon the phasically induced water outflow, reflecting the occurrence of shrinking. The histograms and bar charts compare the start time, namely the delay between hypertonic solution application and rise in SRB fluorescence, the time to reach the peak of shrinking, and the absolute amplitude of water outflow-induced SRB increase ( $n = 58$  astrocytes for CTR, and 47 astrocytes for TGN-020, four mice). (C) *Right*, protocol to trigger water inflow into astrocytes by hypotonic extracellular solution (100 mOsm) in either CTR solution or in the presence of TGN-020 (20  $\mu$ M). (D) Time courses of astrocyte SRB fluorescence decrease caused by water inflow, which also reflects concomitant cell swelling. In contrast to the observation with hypertonicity-induced water outflow and astrocyte shrinking, a reduction was observed for both the start time and the time-to-peak with TGN-020 ( $n = 12$  astrocytes for CTR, and 12 astrocytes for TGN-020, four mice). TGN-020 led to a decrease in the absolute amplitude of astrocyte swelling.

As a post hoc adaptation to the transiently induced Opto-CSD, astrocyte swelling was followed by a shrinking to recover cellular volume to the homeostatic level, which was recorded as a rebound in SRB fluorescence intensity. We noted that TGN-020 presence significantly restrained the recovery of SRB fluorescence back to the baseline (**Fig. 4F** [↗](#), *bottom*), showing that AQP4 inhibition hindered astrocyte water efflux therefore the shrinking.

Collectively, our data show that astrocyte AQP4 sustains a tonic water outflow regulating the cellular volume response and the general cell swelling of the parenchyma.

## Tonic astrocyte water transport underlies brain homeostasis

Water homeostasis sets the basis for molecular diffusion in the brain, which instructs neurotransmitter availability, ion recycling and metabolite trafficking. We then examined *in vivo* the role of astrocyte aquaporin outflow in brain water diffusion using DW-MRI (Le Bihan and Iima, 2015 [↗](#)). It uses the diffusion of water molecules to generate contrast that can be quantified by the apparent diffusion coefficient (ADC) in the nerve tissue (Beaulieu, 2002 [↗](#); Le Bihan, 2014 [↗](#)). We used a 7T MRI to image global brain water diffusion in mice lightly anesthetized with medetomidine that normalized the animals under the sedative state. Astrocyte AQP4 outflow was acutely perturbed by TGN-020 applied via intraperitoneal injection. Brain water diffusion was mapped every 5 min before and after TGN or saline (as control) administration (**Fig. 5A** [↗](#)). Each acquisition sweep was performed with three b values (0, 250, 1800 s/mm<sup>2</sup>) that accounted for ADC, so to fit the exponential curve (**Fig. 5B** [↗](#)). The representative images reveal the enough image quality to calculate the ADC, which allowed us to examine the effect of TGN-020 on water diffusion rate in multiple regions (**Fig. 5C** [↗](#)). The temporal features in water diffusion change appeared also different: an early elevation followed by a reversible tendency was observed for cortical areas, a rapid and long-lasting elevation for the striatum while a delayed and transient increase for the hippocampus (**Fig. 5D** [↗](#), *top*). The respiratory rate was not changed by the injection of TGN020 and saline (Fig. S6). We assessed the time course of ADC change with three phantoms: distilled water, n-undecane, and n-dodecane. Both n-undecane and n-dodecane have been used as phantom for diffusion-weighted image (DWI) (Tofts et al., 2000 [↗](#); Wu and Alexander, 2007 [↗](#)). The ADC was fluctuated within 2% of the averaged ADC at basal period (Fig. S7), indicating that the ADC changes induced by TGN-020 is over the noise level. The *in vivo* neuroimaging results confirm that the tonic water efflux from astrocyte aquaporin contributes to maintain the homeostasis of brain water diffusion, and also suggest spatiotemporal heterogeneities in brain water handling.

## Discussion

Water equilibrium underlies brain function, plasticity and dynamics. Astrocytes are the principal brain cell type expressing aquaporin water channels that are highly implicated in regulating local environments in the parenchyma (Xiao et al., 2023 [↗](#)). We show that albeit being a bidirectional channel, astrocyte aquaporin sustains a tonic water outflow in basal states to ensure structural and functional stability, as well as the water homeostasis at the brain level. We have used the chemical dye SRB to label astrocytes *in vivo*, so as to follow the transmembrane water transport and volume dynamics by real-time fluorescence changes. This sensitivity is ensured by its far lower molecular weight (MW, 558.7 Da), thereby high solubility in the cytoplasm, as compared with fluorescence proteins such as the GFP (MW, 26.9 kDa). In addition, the chemical labeling enables genetics-less targeting of brain astrocytes, so to avoid protein overexpression that may impact astrocyte volume and water transport responses.

The observation of a basal aquaporin water efflux implies there is a constitutive water accumulation in brain astrocytes. As a ubiquitous vehicle for transporting ions, transmitters and metabolites, water enters astrocytes via a wide range of ion channels, transporters and exchangers. For instance, they express Na<sup>+</sup>/K<sup>+</sup> and Na<sup>+</sup>/HCO<sub>3</sub><sup>-</sup> cotransporters to dynamically

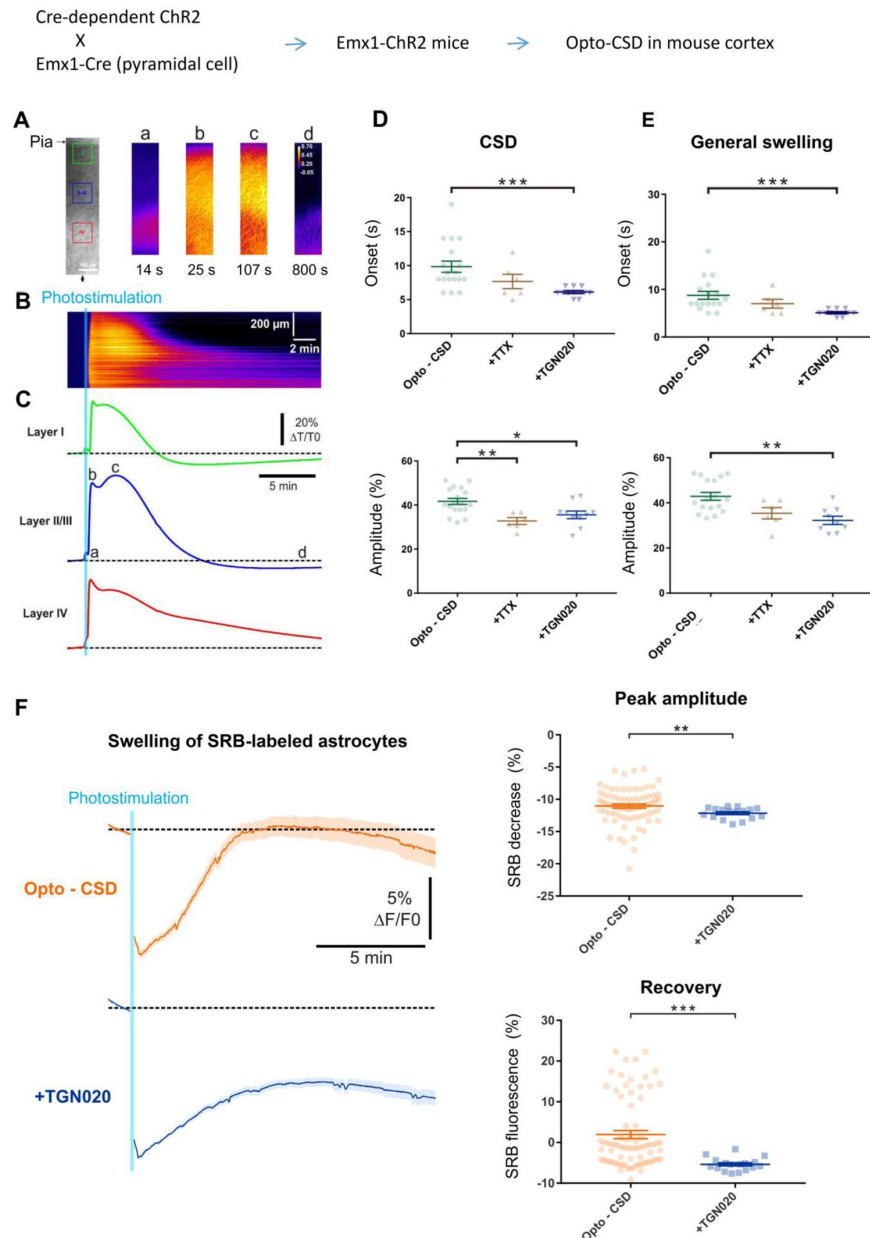


**Fig. 4.**

### AQP4-mediated tonic water outflow regulates global swelling in cortical parenchyma.

CSD-associated general swelling was induced by photostimulating ChR2-expressing pyramidal cells in acute cortical slices, and recorded by imaging intrinsic optical signal (IOS) with infrared illumination. **(A)** Representative recording. The pia surface is on the upper side; green, blue and red squares correspond to regions of interest in Layers I, II-III and IV, respectively. Transmittance signals are represented in pseudocolor images at different time points post photostimulation. Scale bar, 100  $\mu$ m. **(B-C)** Kymograph and time courses showing the IOS changes following photoactivation, derived from the radial line of interest indicated by a black arrow in A. The light blue line indicates the 10-s photostimulation that increases the infrared transmittance signal ( $\Delta T/T_0$ ) across cortical layers, as also illustrated by the time courses; a, b, c and d correspond to the time points depicted in A. After the onset delay (a), the first (b) and second (c) peak of IOS are characteristic of the CSD and a prolonged general swelling, respectively. **(D-E)** TGN-020 (20  $\mu$ M) inhibition of AQP4 reduced the initial onset and the maximal amplitude of both the CSD and general swelling (n = 6 - 18 measurements from 13 mice per condition) in layer II/III cortex. Inhibiting spiking activity with TTX (1  $\mu$ M) only affected the amplitude of the initial CSD response. **(F)** Astrocytes swelling, reflected by SRB fluorescence decrease, monitored in control condition (n = 75 astrocytes) and in the presence of TGN-020 (n = 17 astrocytes) in layer II/III cortex.

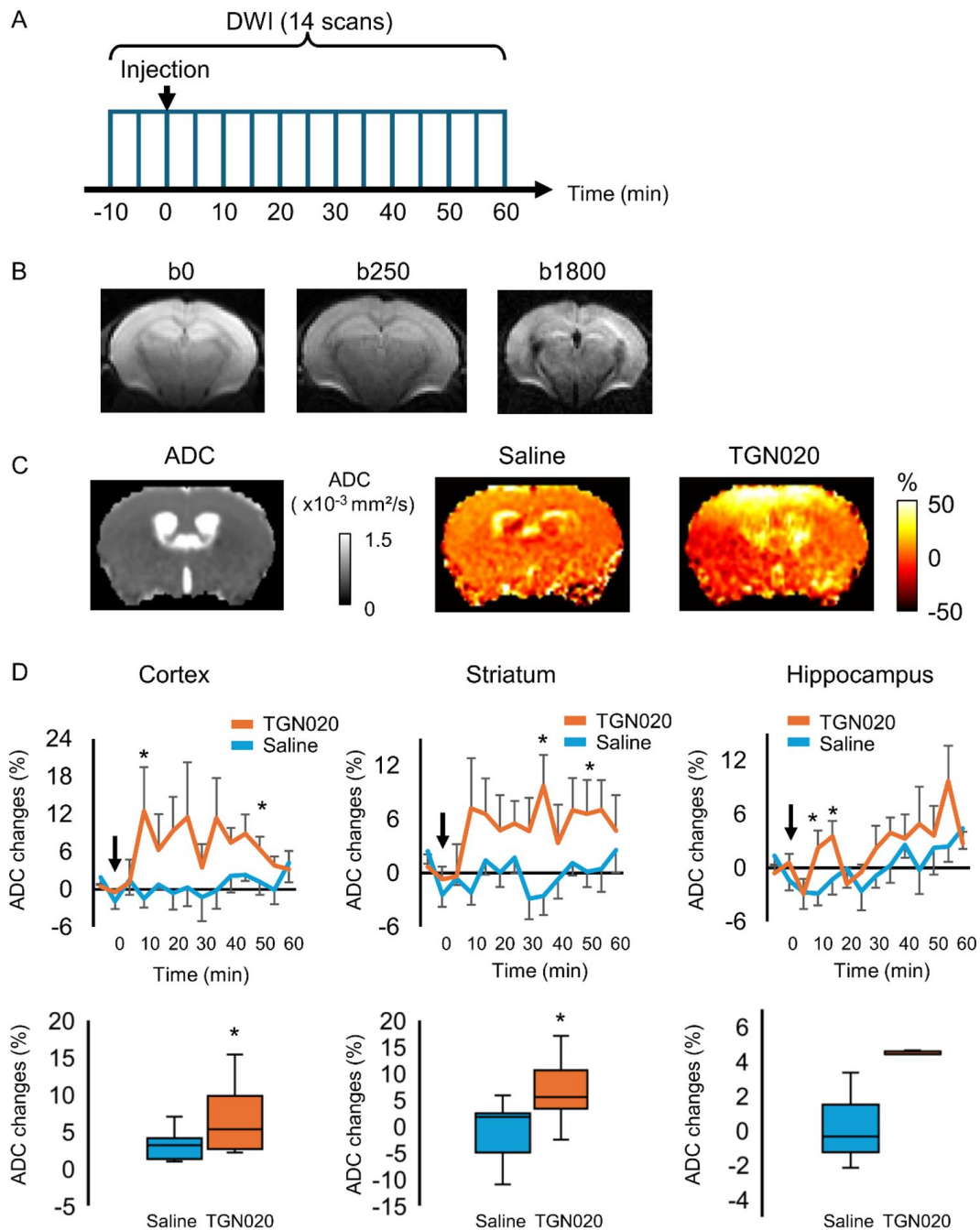


**Fig. 5.**

### Perturbing the tonic water efflux via astrocyte aquaporin alters brain water homeostasis.

*In vivo* DW-MRI (7T) was employed to map water diffusion in the entire brain scale following the acute inhibition of astrocytic AQP4 (TGN-020, intraperitoneal injection, 200 mg/kg), with paralleled control experiments performed with saline injection. (**A**) Experimental protocol for DW-MRI. Saline or TGN020 was injected at 10 min after the start of acquisition. DWI was acquired every 5 min. (**B**) Representative image obtained at three different b values to derive the water diffusion rates. (**C**) *Left*, brain water diffusion rate was mapped by the calculation of apparent diffusion coefficient (ADC). *Right*, representative images illustrating the relative changes of ADC at 60 min after injection of saline or TGN-020. (**D**) *Upper panel*, time courses depicting the temporal changes in ADC in the cortex, striatum, and hippocampus, revealing the regional heterogeneity. Arrowhead indicates the injection of saline or TGN-020 (*n* = 7 mice for saline injection, 7 mice for TGN-020). \**p* < 0.05 vs baseline at each time-point following the two-way repeated measures ANOVA. *Lower panel*, box-plot of the averaged ADC between 30 and 50 min after the injection. \**p* < 0.05 by paired t-test.

regulate intra- and extracellular ion homeostasis (MacAulay, 2021 [↗](#)). Standing as a major glial cell type controlling the neuropil environment, astrocytes take up synaptically released  $K^+$  through inwardly rectified  $K^+$  channels and neurotransmitters (e.g., glutamate, GABA) via high-affinity transporters to safeguard synaptic transmission (Dallerac et al., 2018 [↗](#)). The cotransport of water into the cells with ions or metabolites would lead to water buildup in astrocytes. Moreover, astrocytes juxtapose the cerebral vasculature, being a front relay station for brain metabolism. They express glucose transporters and lactate-permeable monocarboxylate transporters facilitating energy substrate uptake and transfer between blood vessels and neuron-glia networks (Cauli et al., 2023 [↗](#)). As water is constantly produced during metabolic processes (Bonvento and Bolanos, 2021 [↗](#)), astrocyte metabolism would also contribute to the constitutive water accumulation in the cytoplasm. An efficient efflux pathway appears necessary to counterbalance the constitutive water buildup, thereby maintaining astrocyte and brain homeostasis. Our data suggest that astrocyte AQP4 may fulfill such a role by mediating a tonic water outflow (Fig. S8), providing functional evidence to the previous suggestion (Amiry-Moghaddam et al., 2003 [↗](#)). It has been observed that knock out of AQP4 leads to water over accumulation in the brain, likely due to the reduction in water exit from the pial membrane (Haj-Yasein et al., 2011 [↗](#); Vindedal et al., 2016 [↗](#)). Our result also echoes that in the principal cells of the kidney collecting duct, AQP4 is suggested to mainly mediate water exit to balance the AQP2-sustained water entry (Noda et al., 2010 [↗](#)). Moreover, we observed that inhibiting astrocyte basal water efflux alters  $Ca^{2+}$  activities in both astrocytes and neurons, reminiscent of the early finding that inhibition of AQP4 by TGN-020 enhances cerebral blood flow in mouse cortex (Igarashi et al., 2013 [↗](#)), which might be due to the enhanced neuron-astrocyte activity tone. As a pharmacological compound, TGN-020 exerts a partial blocking effect on AQP4 (Huber et al., 2009 [↗](#)), implying that the actual functional impact of AQP4 per se might be stronger than what we currently observed. Alternatively, the phenylbenzamide AER-270 and its water-soluble prodrug AER-271 have been reported as AQP4 blocker (Farr et al., 2019 [↗](#)) and impairs brain water diffusion and glymphatic fluid (Giannetto et al., 2024 [↗](#)). AER270(271) has been noted to also be the inhibitor for  $\kappa B$  nuclear factor (NF- $\kappa B$ ) whose inhibition could reduce CNS water content and influence brain fluid dynamics (e.g., the ADC of DW-MRI) in an AQP4-independent manner (Giannetto et al., 2024 [↗](#); Salman et al., 2022 [↗](#)). The inhibition efficiency of AER-270 seems also lower than that of TGN-020 (Huber et al., 2009 [↗](#); Giannetto et al., 2024 [↗](#); Salman et al., 2022 [↗](#)). Developing pharmacological compounds that can more specifically and efficiently target AQP4 will facilitate the functional and pre-clinical investigations.

This study also provides mechanistic hints to understand AQP4-relevant pathologies in specific contexts. For instance, astrocyte water accumulation and swelling are implicated in the development of brain edema. Different types of edema have been delineated depending on the pathological contexts, including such as cytotoxic, vasogenic and hydrocephalic subtypes. The presence of AQP4 has been found to ameliorate vasogenic (vascular leak) and hydrocephalic edema (Jeon et al., 2021 [↗](#); Tait et al., 2010 [↗](#)), where the excessive water has been suggested to exit the brain via AQP4-dependent route. This goes with our observation that astrocyte AQP4 contributes to basal water extrusion. Hence aquaporin facilitators may help to control vasogenic and hydrocephalic edema. Differently, inhibiting AQP4 has been observed to ameliorate cytotoxic edema encountered during cerebral ischemia (Verkman et al., 2011 [↗](#)). Beneficial effects of TGN-020 on edema have been reported in spinal cord injuries (Li et al., 2019 [↗](#)), in ischemia (Sun et al., 2022 [↗](#)) and in retinal edema in diabetic animal models (Oosuka et al., 2020 [↗](#)). These observations suggest that the role of AQP4 in pathological conditions is context-dependent. Indeed, while our results suggest astrocyte AQP4 mediates a water outflow in basal states, the direction of water transport in specific contexts will be determined by the actual transmembrane water gradient. As the origin of edema is variable and water is among the many other ions involved in edema formation (Stokum et al., 2016 [↗](#)), astrocyte aquaporin may either be the primary cause for cytosolic water accumulation or secondarily sustain protective water extrusion. In neuromyelitis optica spectrum disorders (NMOSD), an unusual nervous autoimmune disorder often featured with circulating IgG autoantibody against AQP4, the impairment in astrocyte water homeostasis

has been observed (Hinson et al., 2012 [↗](#); Lucchinetti et al., 2014 [↗](#)). The inhibition of astrocyte AQP4 by autoantibody may initially affect the basal water efflux. Yet chronic pathological evolution could convert astrocytes into reactive states, with either or both the aquaporin expression, intra- and extracellular environments being altered, the role of AQP4 in water transport might be accordingly shifted (Mireles-Ramirez et al., 2022 [↗](#)). Additionally, pro-inflammatory cytokines and chemokines during the immunological maladaptation could also contribute to shape astrocyte functions including aquaporin-mediated water transport (Lucchinetti et al., 2014 [↗](#); Mireles-Ramirez et al., 2022 [↗](#)). Recent data show that TGN-020 targeting of AQP4 mitigates the inflammation during ischemia-reperfusion injury, by enhancing glymphatic amyloid clearance and inhibiting the ERK 1/2 pathway (Li et al., 2023 [↗](#)), suggesting that in pathological conditions, multiple factors could be recruited by astrocyte aquaporin targeting.

We observed that acutely blocking aquaporin caused basal water accumulation leading to swelling in astrocytes, and facilitated the initial occurrence of the evoked swelling by hypoosmoticity and during cortical spreading depression. This recalls early observation by electron microscopy that knocking out the anchoring protein alpha-syntrophin to disperse AQP4 clustering induces an enlargement of astrocyte end feet (Amiry-Moghaddam et al., 2003 [↗](#)). It likely reflects astrocyte local swelling caused by the disruption of AQP4-mediated water efflux. Our observation also parallels the report that AQP4 knock out facilitates astrocytes swelling induced by hypoosmotic solution (Murphy et al., 2017 [↗](#)). Nevertheless, genetic inactivation of AQP4 also reveals inhibitory effects on astrocyte swelling (Benfenati et al., 2011 [↗](#); Mola et al., 2016 [↗](#); Woo et al., 2018 [↗](#)). Such discrepancy might be due to the variable compensations in brain water content and structure integrity during chronic genetic manipulations (Binder et al., 2004 [↗](#); Haj-Yasein et al., 2011 [↗](#); MacAulay, 2021 [↗](#); Yao et al., 2015 [↗](#)). Using the calcein quenching assay and AQP4 KO (Solenov et al., 2004 [↗](#)), it has been demonstrated in cultured astrocytes that AQP4 is a functional water channel. AQP4 deletion reduced both astrocyte water permeability and the absolute amplitude of swelling over comparable time, and also slowed down cell shrinking, which are overall confirmed by in our results from acute AQP4 blocking. Yet in the study (Solenov et al., 2004 [↗](#)), the time to swelling plateau was prolonged in AQP4 KO astrocytes, which was observed to be accelerated in the present study. This difference may be due to compensatory mechanisms in chronic AQP4 KO, or reflect the different volume responses in cultured astrocytes from brain slices or *in vivo* contexts as noted previously (Risher et al., 2009 [↗](#)). Nevertheless, in the present study, astrocyte volume and water transport dynamics have been inferred from the real-time fluorescence change of SRB labeling. Rapid three-dimensional imaging of astrocyte volume dynamics *in situ* will provide further quantitative information on the role of AQP4 in volume regulations (MacAulay, 2021 [↗](#); MacAulay et al., 2004 [↗](#)). In addition, though our data suggest that under basal condition astrocyte AQP4 sustains a tonic water outflow, in conditions when massive water influx persists as exemplified by the application of hypoosmotic solutions, the direction of water transport of AQP4 would follow the imposed water gradient. Regulatory volume decrease has been observed in cultured astrocyte volume responses behaving as a protective mechanism (Mola et al., 2016 [↗](#)). In current condition in acute brain slices, when we applied hypotonic solution to induce astrocyte swelling, our protocol did not reveal rapid regulatory volume decrease. During opto-CSD, we observed astrocyte volume decrease following the transient swelling (**Fig. 4F** [↗](#)), where both the peak amplitude and the degree of recovery were reduced by inhibiting AQP4 with TGN-020. These observations suggest astrocyte regulatory volume decrease likely to be condition-dependent, while also recalling that the regulatory volume decrease is barely detectable in brain slices or *in vivo* during hypo-osmotic challenge (Risher et al., 2009 [↗](#)). Given the implication of CSD in brain migraine aura, ischemia and seizure (Chung et al., 2019 [↗](#)), the current observation suggests a functional involvement of astrocyte AQP4 in the physiopathological adaptations.

Astrocyte aquaporin modulates brain water transport (MacAulay, 2021 [↗](#)), though its role in the glymphatic system is under deliberation (Mestre et al., 2018a [↗](#); Rasmussen et al., 2022 [↗](#); Smith and Verkman, 2019 [↗](#); Smith et al., 2017 [↗](#)). Our data suggest that astrocyte aquaporin-mediated outflow helps to maintain local water environment in the brain parenchyma, facilitating the

circulation of the interstitial and cerebrospinal fluid. Moreover, besides affecting water transport, targeting AQP4 also impacts astrocyte volume therefore the size of extracellular space. These two factors would need to be considered when evaluating AQP4 involvement in brain fluid transport.

We show by DW-MRI that impairing astrocyte water transport induces the changes of ADC across the brain. When blocking AQP4 with TGN-020, therefore its basal water outflow, we observed spatially heterogeneous elevations in brain water diffusion rate. It has been reported that relative to wild-type mice, AQP4 KO mice show increased water diffusion along with the enlarged interstitial space, brain volume yet reduced CSF spaces (Gomolka et al., 2023 [\[1\]](#)). Notably in AQP4 KO mice, the influx of gadolinium CSF tracer was reduced as followed by dynamic contrast-enhanced MRI (Gomolka et al., 2023 [\[1\]](#)). As corroboration, the AQP4 blocker AER-271 also reduces glymphatic water influx (Giannetto et al., 2024 [\[2\]](#)). Together, these observations suggest that AQP4 plays a critical role not only in modulating water diffusion in brain parenchyma but also in the CSF transport. Our current data are derived from 5 min apart acquisitions, providing information over the early phase of AQP4 inhibition therefore extending our early report (Debacker et al., 2020 [\[3\]](#)). The regional heterogeneity likely reflects the various levels of AQP4 expression; its relative enrichment in the cerebral cortex (Gomolka et al., 2023 [\[1\]](#); Hubbard et al., 2015 [\[4\]](#); Mestre et al., 2018a [\[5\]](#)) corresponds to the pronounced effect observed here by DW-MRI. An overall increase in brain water diffusion rate was observed when blocking AQP4 water efflux. This treatment causes water accumulation inside astrocytes and their swelling, which reduces the extracellular space but increases the intracellular space. Water diffusion would be enhanced inside astrocytes and decreased in extracellular space, respectively. DW-MRI maps global water diffusion of both intra- and extracellular space. Likely, a net increase in brain water diffusion may reflect its intracellular increase exceeding the extracellular decrease. In addition, convective brain fluid flow has been suggested to be present in the perivascular space (Smith and Verkman, 2019 [\[6\]](#)), a scenario extended by the glymphatic system to the extracellular space of the parenchyma (Mestre et al., 2018b [\[7\]](#)). In this sense, transiently squeezing extracellular space might increase the rate of the water flow.

Additionally, a transient upregulation of other water-permeable pathways would increase the water diffusion in compensating the AQP4 blocking. It has been shown that TGN-020 increases regional cerebral blood flow in wild-type mice but not in AQP4 KO mice (Igarashi et al., 2013 [\[8\]](#)). The current MRI data yet lack sufficient spatial resolution to delineate the spatial compartmentalization of brain fluid flow. We here used anisotropic resolution and minimum b-values to earn the temporal resolution. The phantom study supports the quality of DW-MRI data to calculate the time course of ADC. To further use isotropic resolution and more b-values will help to validate our current results.

This study sheds light on the mechanisms by which astrocyte aquaporin contributes to the water environment in brain parenchyma, and will help to understand the processes underlying brain homeostasis and adaptation to life conditions.

## Materials and methods

### Animals and acute brain slice preparation

All procedures using animals were carried out in strict accordance with French regulations (Rural Code R214/87 to R214/130) and conformed to the ethical recommendations of the European Economic Community (Directive 86/609/EEC) and the National Charter French on ethics in animal experimentation. All protocols were approved by the Charles Darwin ethics committee and submitted to the French Ministry of Education and Research (Approval 2015 061011367540 APAFIS#573-2015061011367547 v1).

For water transport and volume imaging, coronal slices comprising somatosensory cortex were acutely prepared from C57BL/6 mice of both sexes at ages of 4–6 weeks, unless otherwise indicated. Mice were deeply anesthetized by isoflurane (ISOVET, Piramal) evaporation in a closed plexiglass box. The brain was taken out and placed in a modified artificial cerebrospinal fluid (aCSF) for slicing (in mM: 30 NaCl, 4.5 KCl, 1.2 NaH<sub>2</sub>PO<sub>4</sub>, 1 MgCl<sub>2</sub>, 26 NaHCO<sub>3</sub>, 10 D-Glucose, and 194 sucrose) maintained at 4 °C during sectioning, where depolarizing ions (Na<sup>+</sup>, Ca<sup>2+</sup>) were reduced in attempt to lower the potential excitotoxicity during the tissue dissection while sucrose used to balance the osmolality (Jiang et al., 2016). The brain was cut into 300-μm thick slices with a vibratome (Leica VT1200S). Brain slices were recovered in standard aCSF (mM: 124 NaCl, 4.5 KCl, 1.2 NaH<sub>2</sub>PO<sub>4</sub>, 1 MgCl<sub>2</sub>, 2 CaCl<sub>2</sub>, 26 NaHCO<sub>3</sub>, and 10 D-Glucose) at 37 °C for about 1 h, and the same aCSF was used for brain slice imaging at room temperature. For optogenetic cortical spreading depression (opto-CSD) experiments, 18 to 21 day-old mice were deeply anesthetized with 150 μL of isoflurane. After the decapitation, the brain was quickly removed and placed into ice-colded oxygenated aCSF containing the following (in mM): NaCl 125; NaHCO<sub>3</sub> 26; Sucrose 15; Glucose 10; KCl 2.5; CaCl<sub>2</sub> 2; NaH<sub>2</sub>PO<sub>4</sub> 1.25; MgCl<sub>2</sub> 1; kynurenic acid 1 (nonspecific glutamate receptor antagonist, Sigma-Aldrich). Coronal slices from mouse somatosensory cortex (300 μm thick) were cut with a vibratome (VT1000, Leica) and allowed to recover at room temperature for at least 45 min in aCSF saturated with O<sub>2</sub>/CO<sub>2</sub> (95%/5%).

### ***In vivo* chemical and genetic targeting of astrocytes**

Mice of similar age were used also for *in vivo* labeling of astrocytes, where the astrocyte-specific red fluorescent dye sulforhodamine B (10 mg/ml, Sigma) was intraperitoneally injected into awake mice at a dose of 10 μL/g. The genetically encoded Ca<sup>2+</sup> indicator GCaMP6 was expressed in astrocytes *in vivo* by crossing a Cre-dependent GCaMP6f mouse line (Ai95, The Jackson Laboratory) with an inducible conditional mouse line *Glast-Cre<sup>ERT2</sup>*, which expresses Cre recombinase selectively in astrocytes upon tamoxifen injection (Slezak et al., 2007). Tamoxifen (T5648, Sigma) was dissolved in 100 % ethanol (10 mg/250 μL). The corn oil (Sigma) was subsequently added at a 9:1 proportion relative to the ethanol-tamoxifen solution. The resultant solution was then heated at 37°C for 15 min, vortexed, sonicated for 15 min to reach transparency, before being aliquoted at 250 μL each containing 1 mg tamoxifen. Aliquots were stored at –20 °C until use. *Glast-Cre<sup>ERT2</sup>::Ai95<sup>GCaMP6f</sup>/WT* mice were injected with tamoxifen at ~3–4 weeks of age, once a day (1 mg) for two consecutive days. Genotyping of the Cre-dependent GCaMP6f mouse line (Ai95, The Jackson Lab) used the standard primers and polymerase chain reaction protocols provided by the supplier. Genotyping of *GLAST-Cre<sup>ERT2</sup>* mouse line was performed using the primers for Cre recombinase (TK139/141) as reported (Slezak et al., 2007). For Ca<sup>2+</sup> imaging in somatostatin interneurons, homozygous mice *B6J.Cg-Sst<sup>tm2.1(cre)Zjh</sup>/MwarJ* (Jackson Laboratory) (Taniguchi et al., 2011) have been crossed with homozygous *Ai95<sup>GCaMP6f</sup>/GCaMP6f* mice to obtain heterozygous *SST-Cre<sup>cre</sup>/WT::Ai95<sup>GCaMP6f</sup>/WT* mice. For opto-CSD, homozygous mice *B6;129Pmx1tm1lr/J* ((Gorski et al., 2002), *Emx1-Cre<sup>cre</sup>/cre*, Jackson Laboratory) have been crossed with homozygous mice *B6;129Sgt(ROSA)26Sortm32.1(CAG-COP4\*H134R/EYFP)Hze/J* ((Madisen et al., 2012), *Ai32<sup>ChR2/ChR2</sup>*, Jackson Laboratory) to obtain heterozygous *Emx1-cre<sup>cre</sup>/WT::Ai32<sup>ChR2/WT</sup>* mice.

### ***Ex vivo* fluorescence imaging**

Light sheet and epifluorescence imaging were both performed using a wide-field upright microscope (Zeiss Axioskop 50, Germany) equipped with water-immersion objectives. Epifluorescence illumination was provided by a monochromator light source (Polychrome II, TILL Photonics, Germany) directly coupled to the imaging objective via an optical fiber. We used water immersion imaging objectives (ZEISS): ×10 NA0.3 used to have a global view, ×20 NA0.5 used to perform light sheet imaging, and ×63 NA1.0 to image individual astrocytes under epifluorescence configuration so as to collect their whole-cell SRB fluorescence to follow astrocyte water transport and volume dynamics. The green fluorescence of GCaMP6 was separated from the red fluorescence of SRB, by spectrally exclusive double-band filters (Di03-R488/561-t3 and FF01-

523/610, Semrock). SRB-labeled astrocytes were excited at 550 nm. Fluorescence signal was collected using a digital electron-multiplying charge-coupled device (EMCCD Cascade 512B, Photometrics).

A light sheet imaging system was adapted from our previous publication (Pham et al., 2020 [DOI](#)), where a chamber with a slightly tilted surface was used so as to spare the agarose embedding and allow the light sheet to access to any parts of the brain slice (Fig. S1). Briefly, the in-focus light sheet was introduced laterally from an independent optical module (Alpha3 light sheet add-on, Phaseview, France) equipped with an air objective (Zeiss EC EPIPlan  $\times 10$ , 0.25NA). This optical module was orthogonal to the upright imaging pathway and coupled via a wavelength combiner (Thorlabs) to two continuous wave lasers 473-nm and 561-nm (CNI, China), for the excitation of GCaMP6 and SRB, respectively. The imaging chamber ( $20 \times 30 \times 46$  mm width, height and length) was custom-designed using 3D modeling software (Trimble SketchUP), produced by a Mojo 3D printer (Stratasys) with the acrylonitrile butadiene styrene material, where the horizontal slice-supporting surface in the chamber was tilted by  $8^\circ$  along the laser entry direction. In this way, the brain slice could be laid on the slightly tilted surface while being stabilized with a conventional Harp slice anchor grid (Warner Instruments), whereby the laterally generated laser light sheet could reach local regions throughout the brain slices. The chamber was mounted on a motorized stage (PI-Physik Instrumente GmbH, Germany) for axial micro-manipulation. Laser excitation and image acquisition were controlled by MetaMorph (Molecular Devices).

Based on the time-lapse image stacks (1 Hz), the active regions of interest (ROIs) of astrocytes displaying dynamic  $\text{Ca}^{2+}$  signals were identified using our established spatio-temporal screening method (Pham et al., 2020 [DOI](#)). The signal strength of astrocyte  $\text{Ca}^{2+}$  signals was estimated from the temporal integral of the normalized  $\text{Ca}^{2+}$  time courses ( $\text{dF}/\text{F}_0$ ,  $\text{F}_0$  is the average of the lowest 20-data point baseline) for the periods prior and post to TGN or vehicle application respectively, which was then normalized per minute. As for neuronal  $\text{Ca}^{2+}$  signals, we followed the global changes with low-frequency imaging (1 Hz) and calculate the mean fluorescence of single  $200 \mu\text{m} \times 200 \mu\text{m}$  field of view. SRB fluorescence dynamics of individual astrocytes was analyzed with ImageJ software (NIH). We sought to follow the temporal changes in SRB fluorescence signal. The acquired fluorescent images contained not only the SRB signal, but also the background signals consisting of, for instance, the biological tissue auto fluorescence, digital camera background noise and the leak light sources from environments. The value of the background signal was estimated by the mean fluorescence of peripheral cell-free subregions ( $15 \times 15 \mu\text{m}^2$ ) and removed from all frames of single time-lapse image stacks.  $\text{F}_0$  was identified as the mean value of the ten data points immediately preceding the detected fluorescence changes, and the same timing used when comparing the paired conditions. Because single astrocytes typically occupy an area of  $\sim 50$ - $100 \mu\text{m}$  in radius (Appaix et al., 2012 [DOI](#)), regions of interest of  $50\text{-}\mu\text{m}$  diameter were delineated surrounding identified astrocyte footprint, to comprise the extended area of individual astrocytes while minimizing interference with neighbors. Time courses extracted from single regions of interest were normalized as  $\text{dF}/\text{F}_0$ .

## Dynamic imaging of the extracellular space and astrocytes volume changes

Individual slices were transferred to a submerged recording chamber and perfused with oxygenated aCSF ( $\sim 2$  ml/min) lacking kynurenic acid. Slices were observed using a double port upright microscope (BX51WI, Olympus, Japan) equipped with Dodt gradient contrast optics (DGC; Luigs and Neumann), collimated light emitting device (LED; 780 nm, Thorlabs) as transmitted light sources,  $\times 4$  objective (PlanN, 0.10NA, Olympus),  $\times 20$  (UMPlanFL N, 0.50 W, Olympus) or  $\times 40$  (LUMPlanF/IR, 0.80 w, Olympus) objectives, and a digital camera (OrcaFlash 4.0, Hamamatsu) attached on the front port of the microscope. The observation with  $\times 4$  allows to delimit the cortical layers and to confirm the presence of “barrels”-like patterns in layer IV (Erzurumlu and Gaspar,

2020 [\[link\]](#)). The  $\times 20$  objective was used to observe infrared intrinsic optical signals (IOS) (Holthoff and Witte, 1996 [\[link\]](#); MacVicar and Hochman, 1991 [\[link\]](#)) of the cortical layers I to IV. The  $\times 40$  objective was used to image SRB labelled astrocytes combined with IOS in layers I and II/III.

After one minute of baseline period, a 10-s continuous photostimulation at 470 nm of the ChR2<sub>H134R</sub> (30% of the maximal power of the LED) was carried out via the epifluorescence port of the microscope using a collimated LED system (CoolLED, PreciseExcite) and a set of multiband filters consisting of an excitation filter (HC 392/474/554/635, Semrock), a dichroic mirror (BS 409/493/573/652, Semrock) and an emission filter (HC 432/515/595/730, Semrock) to observe the induced changes of light transmittance. The infrared and epifluorescence images were acquired each at 1 Hz (exposure 100 ms, binning 2 $\times$ 2) using the Imaging Workbench 6.1 software (Indec Byosystems) for a total duration of 15 min.

### ***In vivo* fiber photometry**

The optical fiber (200  $\mu$ m core, NA = 0.37, Neurophotometrics) coupled to a stainless-steel ferrule (1.25 mm) was stereotactically implanted in mouse S1 cortex (relative to bregma, rostro-caudal 0 mm, lateral  $\pm$  2.5 mm, vertical -1.2mm), and fixed to the skull with dental cement (SuperBond, Sun medical). Mice were familiarized with the setup for 30 minutes prior to fiber photometry recording in mobile states. 5-min baseline was recorded before SRB injection, then SRB was applied to label brain astrocytes via intraperitoneal injection and the fluorescence time course was continuously recorded. To examine *in vivo* the effect on astrocyte water transport of acute AQP4 blocking, either TGN-020 (200 mg/kg; Tocris or MedChemExpress) or saline control was intraperitoneally injected 1 h after SRB injection, a time point when astrocytes were well labeled as confirmed by brain slice imaging.

Fluorescence signals were recorded using a Neurophotometrics fiber photometry system (FP3002). A branched fiber optic patch cord (BFP\_200/230/900-0.37\_FC-MF1.25, Doric Lenses) connected to the fiber photometry apparatus was attached to the implanted fiber optic cannula using a cubic zirconia sleeve. To record fluorescence signals from SRB, excitation light from 560-nm LED was band-pass filtered, collimated, reflected by a dichroic mirror and focused by a  $\times 20$  objective. The excitation light power at the tip of the patch cord was 50  $\mu$ W. Emitted fluorescence was band-pass filtered and focused on digital camera. Signals were collected at a rate of 1 Hz for SRB and visualized using the open-source software Bonsai 2.4 (<http://bonsai-rx.org> [\[link\]](#)) and analyzed in Igor software (Wavemetrics).

### ***In vivo* diffusion-weighted MRI**

To test the effect of astrocyte AQP4 acute inhibition on brain water homeostasis, we used diffusion-weighted magnetic resonance imaging (DW-MRI) to calculate the apparent diffusion coefficient (ADC) of tissue water molecules in the brain. MRI experiment was performed with medetomidine anesthesia (0.6 mg/kg/h, i.v.). Two groups of mice (seven for each) were injected with either the water-soluble TGN-020 sodium salt (Key Organics, LR-0041) or saline. For the crossover test, the order of injection of TGN-020 or saline was randomly determined. The experiment was performed 2 days, which separated 1 month for the recover. The respiration was monitored, and the body temperature was maintained at 36  $^{\circ}$ C throughout the measurement.

The MRI experiments were conducted on a 7.0 tesla MRI system equipped with actively shielded gradients at a maximum strength of 700 mT/m (Biospec; 70/16 Bruker BioSpin, Ettlingen, Germany) and with a cryogenic quadrature radio frequency surface probe (Cryoprobe). We chose the cryoprobe because the signal-to-noise ratio appeared better than volume coil. We also confirmed to obtain good image quality in whole brain (**Fig. 5B-C** [\[link\]](#)). After 10 min from the start of the scanning, either TGN-020 (200 mg/kg body weight) or Saline was injected. Then, scanning was continued for 60 min. The respiration rate was monitored and was confirmed within the range of 80-150 / min throughout the experiment. Mice were injected with 200 mg/kg of TGN-020. We used a

standard diffusion-weighted spin echo EPI sequence, with the following parameters: spatial resolution =  $175 \times 175 \times 500 \mu\text{m}^3/\text{voxel}$ , 3 b-values ( $b = 0, 250$  and  $1800 \text{ s/mm}^2$ ), 6 directions, 1 segment, echo time = 37.1 ms / repetition time = 5769 ms, bandwidth = 300 kHz,  $\delta = 3 \text{ ms}$ ,  $\Delta = 24 \text{ ms}$ , scan time = 5 min. The DWI scan was continued for 70 min (total 14 scans). We used minimum direction of motion probing gradient and anisotropic resolution to image the time course of ADC changes following the injection of the TGN-020 (Debacker et al., 2020 [DOI](#)). Previous study has used long diffusion time ( $> 20 \text{ ms}$ ) and long echo time (40 ms) to follow the mean diffusivity (Aggarwal et al., 2020 [DOI](#)), supporting the suitability of our protocol to investigate the ADC. The stability of DW-MRI was evaluated through 70-minute scans using three different phantoms: water, n-undecane (Merck, Darmstadt, Germany), and n-dodecane (Merck, Darmstadt, Germany).

The motion correction of DWI data was performed using statistical parametric mapping software (SPM12, Wellcome Trust Center for Neuroimaging, UK). The template image and regions of interest (ROIs) were then co-registered to the DWI data using SPM12. The ROIs of the cortex, the hippocampus, and the striatum were depicted with reference to Allen mouse brain atlas (<https://scalablebrainatlas.incf.org/mouse/ABA12> [DOI](#)). The ADC at each time point was calculated from DWI data with all b-values ( $b = 0, 250$ , and  $1800 \text{ s/mm}^2$ ) using DSIstudio (<https://dsi-studio.labsolver.org> [DOI](#)). The percentage change in ADC was then calculated according to the equation:  $\Delta\text{ADC}_i = (\text{ADC}_i / \text{ADC}_2 - 1) \times 100 (\%)$ . The  $\text{ADC}_i$  is the ADC at the  $i$ -th time point. We define the averaged ADC at 1<sup>st</sup> and 2<sup>nd</sup> time-point as the baseline because saline injection was performed after the 2<sup>nd</sup> DWI scan. The averaged ADC changes within ROIs were calculated using a homemade program.

## Statistics

Experimental data are expressed as mean  $\pm$  standard error unless otherwise mentioned. The  $t$ -test was performed for two-group comparisons and significant difference was determined by  $p$  values less than 0.05. Mann-Whitney U test was used when the data were non-parametric deviating from normal distributions. Bonferroni-Holm correction was used for multiple comparisons. Statistical tests were carried out with Matlab (The MathWorks) and Statistica 6 (Statsoft). The significance levels are shown in figures by  $*p < 0.05$ ,  $**p < 0.01$ ,  $***p < 0.001$ .

## Acknowledgements

We thank the animal and imaging facilities of the IBPS (Sorbonne Université, Paris, France). We thank Nathalie Rouach for the GFAP-EGFP mice, Hervé Le Corronc and Thomas Panier for the discussion and the 3D printing of the light sheet chamber, respectively. This work was supported by the Agence Nationale de la Recherche (ANR-17-CE37-0010-03; ANR-20-CE14-0025-02), Japanese society for promotion of science (JSPS) 2022 summer grant, Grant-in-Aid for Challenging Research (Exploratory) in Japan (grant number 21K19464), the i-Bio initiative grant and the Emergence program of Sorbonne Université, and the grant from the Fondation de France. CP was supported by a fellowship from France Alzheimer and BLG by a fellowship from the Fondation pour la Recherche sur Alzheimer.

## Competing interest

The authors declare no competing financial interests.

## Data availability

The authors commit to share data, documentation, and code used in analysis.

## References

- Abbott N.J., Pizzo M.E., Preston J.E., Janigro D., Thorne R.G (2018) **The role of brain barriers in fluid movement in the CNS: is there a 'glymphatic' system?** *Acta Neuropathol* **135**:387–407
- Aggarwal M., Smith M.D., Calabresi P.A (2020) **Diffusion-time dependence of diffusional kurtosis in the mouse brain** *Magn Reson Med* **84**:1564–1578
- Agnati L.F., Marcoli M., Leo G., Maura G., Guidolin D (2017) **Homeostasis and the concept of 'interstitial fluids hierarchy': Relevance of cerebrospinal fluid sodium concentrations and brain temperature control (Review)** *Int J Mol Med* **39**:487–497
- Amiry-Moghaddam M. *et al.* (2003) **An alpha-syntrophin-dependent pool of AQP4 in astroglial end-feet confers bidirectional water flow between blood and brain** *Proceedings of the National Academy of Sciences of the United States of America* **100**:2106–2111
- Appaix F., Girod S., Boisseau S., Romer J., Vial J.C., Albrieux M., Maurin M., Depaulis A., Guillemain I., van der Sanden B. (2012) **Specific in vivo staining of astrocytes in the whole brain after intravenous injection of sulforhodamine dyes** *PLoS One* **7**
- Barres B.A (2008) **The mystery and magic of glia: a perspective on their roles in health and disease** *Neuron* **60**:430–440
- Beaulieu C (2002) **The basis of anisotropic water diffusion in the nervous system - a technical review** *NMR Biomed* **15**:435–455
- Benfenati V., Caprini M., Dovizio M., Mylonakou M.N., Ferroni S., Ottersen O.P., Amiry-Moghaddam M (2011) **An aquaporin-4/transient receptor potential vanilloid 4 (AQP4/TRPV4) complex is essential for cell-volume control in astrocytes** *Proceedings of the National Academy of Sciences of the United States of America* **108**:2563–2568
- Binder D.K., Papadopoulos M.C., Haggie P.M., Verkman A.S (2004) **In vivo measurement of brain extracellular space diffusion by cortical surface photobleaching** *J Neurosci* **24**:8049–8056
- Bonvento G., Bolanos J.P (2021) **Astrocyte-neuron metabolic cooperation shapes brain activity** *Cell metabolism* **33**:1546–1564
- Brinker T., Stopa E., Morrison J., Klinge P (2014) **A new look at cerebrospinal fluid circulation** *Fluids Barriers CNS* **11**
- Burnett M.E., Johnston H.M., Green K.N (2015) **Structural characterization of the aquaporin inhibitor 2-nicotinamido-1,3,4-thiadiazole** *Acta Crystallogr C Struct Chem* **71**:1074–1079
- Cauli B., Dusart I., Li D (2023) **Lactate as a determinant of neuronal excitability, neuroenergetics and beyond** *Neurobiol Dis* **184**
- Cauli B., Porter J.T., Tsuzuki K., Lambolez B., Rossier J., Quenet B., Audinat E (2000) **Classification of fusiform neocortical interneurons based on unsupervised clustering** *Proceedings of the National Academy of Sciences of the United States of America* **97**:6144–6149

- Chung D.Y. *et al.* (2019) **Determinants of Optogenetic Cortical Spreading Depolarizations** *Cereb Cortex* **29**:1150–1161
- Dallerac G., Zapata J., Rouach N (2018) **Versatile control of synaptic circuits by astrocytes: where, when and how?** *Nat Rev Neurosci* **19**:729–743
- Debacker C., Djemai B., Ciobanu L., Tsurugizawa T., Le Bihan D. (2020) **Diffusion MRI reveals in vivo and non-invasively changes in astrocyte function induced by an aquaporin-4 inhibitor** *PLoS One* **15**
- Eilert-Olsen M., Hjukse J.B., Thoren A.E., Tang W., Enger R., Jensen V., Pettersen K.H., Nagelhus E.A (2019) **Astroglial endfeet exhibit distinct Ca(2+) signals during hypoosmotic conditions** *Glia* **67**:2399–2409
- Erzurumlu R.S., Gaspar P (2020) **How the Barrel Cortex Became a Working Model for Developmental Plasticity: A Historical Perspective** *J Neurosci* **40**:6460–6473
- Farr G.W. *et al.* (2019) **Functionalized Phenylbenzamides Inhibit Aquaporin-4 Reducing Cerebral Edema and Improving Outcome in Two Models of CNS Injury** *Neuroscience* **404**:484–498
- Fiacco T.A., Agulhon C., Taves S.R., Petravic J., Casper K.B., Dong X., Chen J., McCarthy K.D (2007) **Selective stimulation of astrocyte calcium in situ does not affect neuronal excitatory synaptic activity** *Neuron* **54**:611–626
- Gaddamanugu S., Shafaat O., Sotoudeh H., Sarrami A.H., Rezaei A., Saadatpour Z., Singhal A (2022) **Clinical applications of diffusion-weighted sequence in brain imaging: beyond stroke** *Neuroradiology* **64**:15–30
- Giannetto M.J., Gomolka R.S., Gahn-Martinez D., Newbold E.J., Bork P.A.R., Chang E., Gresser M., Thompson T., Mori Y., Nedergaard M (2024) **Glymphatic fluid transport is suppressed by the aquaporin-4 inhibitor AER-271** *Glia*
- Gomolka R.S. *et al.* (2023) **Loss of aquaporin-4 results in glymphatic system dysfunction via brain-wide interstitial fluid stagnation** *eLife* **12**
- Gorski J.A., Talley T., Qiu M., Puelles L., Rubenstein J.L., Jones K.R (2002) **Cortical excitatory neurons and glia, but not GABAergic neurons, are produced in the Emx1-expressing lineage** *J Neurosci* **22**:6309–6314
- Hablit L.M., Pla V., Giannetto M., Vinitsky H.S., Staeger F.F., Metcalfe T., Nguyen R., Benraiss A., Nedergaard M (2020) **Circadian control of brain glymphatic and lymphatic fluid flow** *Nature communications* **11**
- Haj-Yasein N.N. *et al.* (2011) **Glial-conditional deletion of aquaporin-4 (Aqp4) reduces blood-brain water uptake and confers barrier function on perivascular astrocyte endfeet** *Proceedings of the National Academy of Sciences of the United States of America* **108**:17815–17820
- Harrison I.F. *et al.* (2020) **Impaired glymphatic function and clearance of tau in an Alzheimer's disease model** *Brain* **143**:2576–2593
- Herrera Moro Chao D. *et al.* (2022) **Hypothalamic astrocytes control systemic glucose metabolism and energy balance** *Cell metabolism* **34**:1532–1547

- Hinson S.R., Romero M.F., Popescu B.F., Lucchinetti C.F., Fryer J.P., Wolburg H., Fallier-Becker P., Noell S., Lennon V.A (2012) **Molecular outcomes of neuromyelitis optica (NMO)-IgG binding to aquaporin-4 in astrocytes** *Proceedings of the National Academy of Sciences of the United States of America* **109**:1245–1250
- Holthoff K., Witte O.W (1996) **Intrinsic optical signals in rat neocortical slices measured with near-infrared dark-field microscopy reveal changes in extracellular space** *J Neurosci* **16**:2740–2749
- Hubbard J.A., Hsu M.S., Seldin M.M., Binder D.K (2015) **Expression of the Astrocyte Water Channel Aquaporin-4 in the Mouse Brain** *ASN Neuro* **7**
- Huber V.J., Tsujita M., Nakada T (2009) **Identification of aquaporin 4 inhibitors using in vitro and in silico methods** *Bioorg Med Chem* **17**:411–417
- Igarashi H., Huber V.J., Tsujita M., Nakada T (2011) **Pretreatment with a novel aquaporin 4 inhibitor, TGN-020, significantly reduces ischemic cerebral edema** *Neurol Sci* **32**:113–116
- Igarashi H., Tsujita M., Suzuki Y., Kwee I.L., Nakada T (2013) **Inhibition of aquaporin-4 significantly increases regional cerebral blood flow** *Neuroreport* **24**:324–328
- Iloff J.J., Lee H., Yu M., Feng T., Logan J., Nedergaard M., Benveniste H (2013) **Brain-wide pathway for waste clearance captured by contrast-enhanced MRI** *J Clin Invest* **123**:1299–1309
- Iloff J.J. *et al.* (2012) **A paravascular pathway facilitates CSF flow through the brain parenchyma and the clearance of interstitial solutes, including amyloid beta** *Sci Transl Med* **4**
- Jeon H. *et al.* (2021) **Upregulation of AQP4 Improves Blood-Brain Barrier Integrity and Perihematomal Edema Following Intracerebral Hemorrhage** *Neurotherapeutics* **18**:2692–2706
- Jiang R., Diaz-Castro B., Looger L.L., Khakh B.S (2016) **Dysfunctional Calcium and Glutamate Signaling in Striatal Astrocytes from Huntington’s Disease Model Mice** *J Neurosci* **36**:3453–3470
- Karagiannis A. *et al.* (2021) **Lactate is an energy substrate for rodent cortical neurons and enhances their firing activity** *eLife* **10**
- Kimelberg H.K (2004) **Water homeostasis in the brain: basic concepts** *Neuroscience* **129**:851–860
- Kress B.T. *et al.* (2014) **Impairment of paravascular clearance pathways in the aging brain** *Ann Neurol* **76**:845–861
- Le Bihan D. (2014) **Diffusion MRI: what water tells us about the brain** *EMBO Mol Med* **6**:569–573
- Le Bihan D., Iima M. (2015) **Diffusion Magnetic Resonance Imaging: What Water Tells Us about Biological Tissues** *PLoS Biol* **13**

- Le Bihan D., Urayama S., Aso T., Hanakawa T., Fukuyama H. (2006) **Direct and fast detection of neuronal activation in the human brain with diffusion MRI** *Proceedings of the National Academy of Sciences of the United States of America* **103**:8263–8268
- Li J., Jia Z., Xu W., Guo W., Zhang M., Bi J., Cao Y., Fan Z., Li G (2019) **TGN-020 alleviates edema and inhibits astrocyte activation and glial scar formation after spinal cord compression injury in rats** *Life sciences* **222**:148–157
- Li X. *et al.* (2023) **TGN-020 Alleviate Inflammation and Apoptosis After Cerebral Ischemia-Reperfusion Injury in Mice Through Glymphatic and ERK1/2 Signaling Pathway** *Mol Neurobiol*
- Lucchinetti C.F., Guo Y., Popescu B.F., Fujihara K., Itoyama Y., Misu T (2014) **The pathology of an autoimmune astrocytopathy: lessons learned from neuromyelitis optica** *Brain Pathol* **24**:83–97
- MacAulay N (2021) **Molecular mechanisms of brain water transport** *Nat Rev Neurosci* **22**:326–344
- MacAulay N., Hamann S., Zeuthen T (2004) **Water transport in the brain: role of cotransporters** *Neuroscience* **129**:1031–1044
- MacVicar B.A., Hochman D (1991) **Imaging of synaptically evoked intrinsic optical signals in hippocampal slices** *J Neurosci* **11**:1458–1469
- Madisen L. *et al.* (2012) **A toolbox of Cre-dependent optogenetic transgenic mice for light-induced activation and silencing** *Nat Neurosci* **15**:793–802
- Mestre H. *et al.* (2018) **Aquaporin-4-dependent glymphatic solute transport in the rodent brain** *eLife* **7**
- Mestre H., Tithof J., Du T., Song W., Peng W., Sweeney A.M., Olveda G., Thomas J.H., Nedergaard M., Kelley D.H (2018) **Flow of cerebrospinal fluid is driven by arterial pulsations and is reduced in hypertension** *Nature communications* **9**
- Mireles-Ramirez M.A., Pacheco-Moises F.P., Gonzalez-Usigli H.A., Sanchez-Rosales N.A., Hernandez-Preciado M.R., Delgado-Lara D.L.C., Hernandez-Cruz J.J., Ortiz G.G (2022) **Neuromyelitis optica spectrum disorder: pathophysiological approach** *Int J Neurosci* :1–13
- Mola M.G., Sparaneo A., Gargano C.D., Spray D.C., Svelto M., Frigeri A., Scemes E., Nicchia G.P (2016) **The speed of swelling kinetics modulates cell volume regulation and calcium signaling in astrocytes: A different point of view on the role of aquaporins** *Glia* **64**:139–154
- Murphy T.R., Davila D., Cuvelier N., Young L.R., Lauderdale K., Binder D.K., Fiacco T.A (2017) **Hippocampal and Cortical Pyramidal Neurons Swell in Parallel with Astrocytes during Acute Hypoosmolar Stress** *Front Cell Neurosci* **11**
- Noda Y., Sohara E., Ohta E., Sasaki S (2010) **Aquaporins in kidney pathophysiology** *Nat Rev Nephrol* **6**:168–178
- Ochoa-de la Paz L.D., Gullias-Canizo R. (2022) **Glia as a key factor in cell volume regulation processes of the central nervous system** *Front Cell Neurosci* **16**

- Oosuka S., Kida T., Oku H., Horie T., Morishita S., Fukumoto M., Sato T., Ikeda T (2020) **Effects of an Aquaporin 4 Inhibitor, TGN-020, on Murine Diabetic Retina** *Int J Mol Sci* **21**
- Papadopoulos M.C., Verkman A.S (2013) **Aquaporin water channels in the nervous system** *Nat Rev Neurosci* **14**:265–277
- Pham C. *et al.* (2020) **Mapping astrocyte activity domains by light sheet imaging and spatio-temporal correlation screening** *Neuroimage* **220**
- Rasmussen M.K., Mestre H., Nedergaard M (2022) **Fluid transport in the brain** *Physiol Rev* **102**:1025–1151
- Risher W.C., Andrew R.D., Kirov S.A (2009) **Real-time passive volume responses of astrocytes to acute osmotic and ischemic stress in cortical slices and in vivo revealed by two-photon microscopy** *Glia* **57**:207–221
- Salman M.M., Kitchen P., Yool A.J., Bill R.M (2022) **Recent breakthroughs and future directions in druging aquaporins** *Trends Pharmacol Sci* **43**:30–42
- Slezak M., Goritz C., Niemiec A., Frisen J., Chambon P., Metzger D., Pfrieger F.W (2007) **Transgenic mice for conditional gene manipulation in astroglial cells** *Glia* **55**:1565–1576
- Smith A.J., Verkman A.S (2019) **CrossTalk opposing view: Going against the flow: interstitial solute transport in brain is diffusive and aquaporin-4 independent** *J Physiol* **597**:4421–4424
- Smith A.J., Yao X., Dix J.A., Jin B.J., Verkman A.S (2017) **Test of the ‘glymphatic’ hypothesis demonstrates diffusive and aquaporin-4-independent solute transport in rodent brain parenchyma** *eLife* **6**
- Solenov E., Watanabe H., Manley G.T., Verkman A.S (2004) **Sevenfold-reduced osmotic water permeability in primary astrocyte cultures from AQP-4-deficient mice, measured by a fluorescence quenching method** *Am J Physiol Cell Physiol* **286**:C426–432
- Stokum J.A., Gerzanich V., Simard J.M (2016) **Molecular pathophysiology of cerebral edema** *Journal of cerebral blood flow and metabolism: official journal of the International Society of Cerebral Blood Flow and Metabolism* **36**:513–538
- Sun C., Lin L., Yin L., Hao X., Tian J., Zhang X., Ren Y., Li C., Yang Y (2022) **Acutely Inhibiting AQP4 With TGN-020 Improves Functional Outcome by Attenuating Edema and Peri-Infarct Astrogliosis After Cerebral Ischemia** *Front Immunol* **13**
- Tait M.J., Saadoun S., Bell B.A., Verkman A.S., Papadopoulos M.C (2010) **Increased brain edema in aqp4-null mice in an experimental model of subarachnoid hemorrhage** *Neuroscience* **167**:60–67
- Taniguchi H. *et al.* (2011) **A resource of Cre driver lines for genetic targeting of GABAergic neurons in cerebral cortex** *Neuron* **71**:995–1013
- Toft-Bertelsen T.L., Larsen B.R., Christensen S.K., Khandelia H., Waagepetersen H.S., MacAulay N (2021) **Clearance of activity-evoked K(+) transients and associated glia cell swelling occur independently of AQP4: A study with an isoform-selective AQP4 inhibitor** *Glia* **69**:28–41

- Tofts P.S., Lloyd D., Clark C.A., Barker G.J., Parker G.J., McConville P., Baldock C., Pope J.M (2000) **Test liquids for quantitative MRI measurements of self-diffusion coefficient in vivo** *Magn Reson Med* **43**:368–374
- Tsurugizawa T., Ciobanu L., Le Bihan D. (2013) **Water diffusion in brain cortex closely tracks underlying neuronal activity** *Proceedings of the National Academy of Sciences of the United States of America* **110**:11636–11641
- Verkman A.S., Ratelade J., Rossi A., Zhang H., Tradtrantip L (2011) **Aquaporin-4: orthogonal array assembly, CNS functions, and role in neuromyelitis optica** *Acta Pharmacol Sin* **32**:702–710
- Verkman A.S., Smith A.J., Phuan P.W., Tradtrantip L., Anderson M.O (2017) **The aquaporin-4 water channel as a potential drug target in neurological disorders** *Expert opinion on therapeutic targets* **21**:1161–1170
- Vindedal G.F., Thoren A.E., Jensen V., Klungland A., Zhang Y., Holtzman M.J., Ottersen O.P., Nagelhus E.A (2016) **Removal of aquaporin-4 from glial and ependymal membranes causes brain water accumulation** *Mol Cell Neurosci* **77**:47–52
- Woo J. *et al.* (2018) **Astrocytic water channel aquaporin-4 modulates brain plasticity in both mice and humans: a potential gliogenetic mechanism underlying language-associated learning** *Mol Psychiatry* **23**:1021–1030
- Wu Y.C., Alexander A.L (2007) **A method for calibrating diffusion gradients in diffusion tensor imaging** *J Comput Assist Tomogr* **31**:984–993
- Xiao M., Hou J., Xu M., Li S., Yang B (2023) **Aquaporins in Nervous System** *Adv Exp Med Biol* **1398**:99–124
- Yang J., Vitery M.D.C., Chen J., Osei-Owusu J., Chu J., Qiu Z (2019) **Glutamate-Releasing SWELL1 Channel in Astrocytes Modulates Synaptic Transmission and Promotes Brain Damage in Stroke** *Neuron*
- Yao X., Smith A.J., Jin B.J., Zador Z., Manley G.T., Verkman A.S (2015) **Aquaporin-4 regulates the velocity and frequency of cortical spreading depression in mice** *Glia* **63**:1860–1869
- Zhao H.H., Du H., Cai Y., Liu C., Xie Z., Chen K.C (2019) **Time-resolved quantification of the dynamic extracellular space in the brain: study of cortical spreading depression** *Journal of neurophysiology* **121**:1735–1747

## Editors

Reviewing Editor

**Annalisa Scimemi**

University at Albany, State University of New York, Albany, United States of America

Senior Editor

**John Huguenard**

Stanford University School of Medicine, Stanford, United States of America

**Reviewer #1 (Public review):****Summary:**

Pham and colleagues provide an illuminating investigation of aquaporin-4 water flux in the brain utilizing ex vivo and in vivo techniques. The authors first show in acute brain slices, and in vivo with fiber photometry, SRB loaded astrocytes swell after inhibition of AQP4 with TGN-020, indicative of tonic water efflux from astrocytes in physiological conditions. Excitingly, they find that TGN-020 increased the ADC in DW-MRI in a region-specific manner, potentially due to AQP4 density. The resolution of the DW-MRI cannot distinguish between intracellular or extracellular compartments, but the data point to an overall accumulation of water in the brain with AQP4 inhibition. These results provide further clarity on water movement through AQP4 in health and disease.

Overall, the data support the main conclusions of the article, with some room for more detailed treatment of the data to extend the findings.

**Strengths:**

The authors have a thorough investigation of AQP4 inhibition in acute brain slices. The demonstration of tonic water efflux through AQP4 at baseline is novel and important in and of itself. Their further testing of TGN-020 in hyper- and hypo-osmotic solutions shows the expected reduction of swelling/shrinking with AQP4 blockade.

Their experiment with cortical spreading depression further highlights the importance of water efflux from astrocytes via AQP4 and transient water fluxes as a result of osmotic gradients. Inhibition of AQP4 increases the speed of tissue swelling, pointing to a role in efflux of water from the brain.

The use of DW-MRI provides a non-invasive measure of water flux after TGN-020 treatment.

**Weaknesses:**

The authors specifically use GCaMP6 and light sheet microscopy to image their brain sections in order to identify astrocytic microdomains. However, their presentation of the data neglects a more detailed treatment of the calcium signaling. It would be quite interesting to see whether these calcium events are differentially affected by AQP4 inhibition based on their cellular localization (ie. processes vs. soma vs. vascular endfeet which all have different AQP4 expression).

The authors show the inhibition of AQP4 with TGN-020 shortens the onset time of the swelling associated with cortical spreading depression in brain slices. However, they do not show quantification for much of the other features of the CSD swelling, (ie. the duration of swelling, speed of swelling, recovery from swelling)

**Comments on revised version:**

The authors have addressed these suggestions as additional supplementary figures. Notably they find increased calcium signaling and stronger inhibition of calcium signaling by TGN-020 in astrocytic endfeet, where AQP4 is enriched.

**Significance:**

AQP4 is a bidirectional water channel that is constitutively open, thus water flux through it is always regulated by local osmotic gradients. Still, characterizing this water flux has been challenging, as the AQP4 channel is incredibly water selective. The authors here present important data showing that application of TGN-020 alone causes astrocytic swelling, indicating that there is constant efflux of water from astrocytes via AQP4 in basal conditions.

This has been suggested before, as the authors rightfully highlight in their discussion, but the evidence had previously come from electron microscopy data from genetic knockout mice.

AQP4 expression has been linked with glymphatic circulation of cerebrospinal fluid through perivascular spaces since its rediscovery in 2012 [1]. Further studies of aging[2], genetic models[3], and physiological circadian variation[4], have revealed it is not simply AQP4 expression but AQP4 polarization to astrocytic vascular endfeet that is imperative for facilitating glymphatic flow. Still a lingering question in the field is how AQP4 facilitates fluid circulation. This study represents an important step in our understanding of AQP4's function, as basal efflux of water via AQP4 might promote clearance of interstitial fluid to allow influx of cerebrospinal fluid into the brain. Beyond glymphatic fluid circulation, clearly AQP4 dependent volume changes will differentially alter astrocytic calcium signaling and, in turn, neuronal activity.

- (1) Iliff, J.J., et al., A Paravascular Pathway Facilitates CSF Flow Through the Brain Parenchyma and the Clearance of Interstitial Solutes, Including Amyloid  $\beta$ . *Sci Transl Med*, 2012. 4(147): p. 147ra111.
- (2) Kress, B.T., et al., Impairment of paravascular clearance pathways in the aging brain. *Ann Neurol*, 2014. 76(6): p. 845-61.
- (3) Mestre, H., et al., Aquaporin-4-dependent Glymphatic Solute Transport in the Rodent Brain. *eLife*, 2018. 7.
- (4) Hablitz, L., et al., Circadian control of brain glymphatic and lymphatic fluid flow. *Nature communications*, 2020. 11(1).

<https://doi.org/10.7554/eLife.95873.2.sa2>

### Reviewer #3 (Public review):

#### Summary:

In this manuscript, the Authors propose that astrocytic water channel AQP4 represents the dominant pathway for tonic water efflux without which astrocytes undergo cell swelling. The authors measure changes in astrocytic sulforhodamine B fluorescence as the proxy for cell volume dynamics. Using this approach, they have performed a technically elegant series of ex vivo and in vivo experiments exploring changes in astrocytic volume "signal" in response to the AQP4 inhibitor TGN-020 and/or neuronal stimulation. The key findings are that TGN-020 produces an apparent swelling of astrocytes and modifies astrocytic cell volume dynamics after spreading depolarizations. This study is perceived as potentially highly significant. However, several technical caveats could be considered better and perhaps addressed through additional experiments.

#### Strengths:

- (1) This is a technically sound study, in which the Authors employed a number of complementary ex vivo and in vivo techniques. The presented results are of interest to the field and potentially highly significant.
- (2) The innovative use of sulforhodamine B for in situ measurements of astrocyte cell volume dynamics is thoroughly validated in brain slices by quantifying changes in sulforhodamine fluorescence in response to hypoosmotic and hyperosmotic media.
- (3) The combination of cell volume measurements with registering functional outcomes in both astrocytes and neurons (cell-specific GCaMP6 signaling) is appropriate and adds to the significance of the work.

(4) The use of Chr2 optogenetics for producing spreading depolarization allows to avoid many complications of chemical manipulations and much appreciated.

Remaining limitations:

(1) In the opinion of this reviewer, the effects of TGN-020 are not entirely consistent with the current knowledge on water permeability in astrocytes and the relative contribution of AQP4 to this process.

Specifically, genetic deletion of AQP4 reduces plasmalemmal water permeability in astrocytes by ~two-three-fold (when measured at 37°C, E. Solenov et al., *AJP-Cell*, 2004). This difference is significant but thought to have limited impact on steady-state water distribution. To the best of this reviewer's knowledge, cultured AQP4-null astrocytes do not show changes in degree of hypoosmotic swelling or hyperosmotic shrinkage. Thus, the findings of Solenov et al. are not (entirely) congruent with the conclusions of the current manuscript.

Also, as noted by the Authors, the AQP4 knockout does not modify astrocytes swelling induced by hypoosmotic solution in brain slices (T.R. Murphy et al., *Front Neurosci.*, 2017), further suggesting that AQP4 is not a significant rate-limiting factor for water movement across astrocyte membranes.

The Authors do discuss the above-mentioned discrepancies and explain them by the context-dependent changes in water fluxes. Nevertheless, with these caveats in mind, it would be highly desirable to utilize an independent method measuring astrocytic volume and extracellular volume fraction.

(2) As noted by this reviewer and now discussed by the Authors, changes in ADC signal (presented in in Fig. 5) may be confounded by the previously reported TGN-020-induced hyphemia (e.g., H. Igarashi et al., *NeuroReport*, 2013) and/or changes water fluxes across pia matter which is highly enriched in AQP4. If this is the case, the proposed brain water accumulation may be explained by factors other than astrocytic water homeostasis. This caveat certainly deserves further experimental exploration.

<https://doi.org/10.7554/eLife.95873.2.sa1>

#### Author response:

The following is the authors' response to the current reviews.

Many thanks to the editors for the reviewing of the revised manuscript.

We are very grateful to the Reviewers for their time and for the appreciation of the revision.

We thank the Reviewer 3 for acknowledging the use of sulforhodamine B (SRB) fluorescence as a real-time readout of astrocyte volume dynamics. Experimental data in brain slices were provided to validate this approach.

The incomplete matching of our observation with early reported data in cultured astrocytes (e.g., Solenov et al., *AJP-Cell*, 2004), might reflect certain of their properties differing from the slice/in vivo counterparts as discussed in the manuscript.

The study (T.R. Murphy et al., *Front Cell Neurosci.*, 2017) showed that AQP4 knockout increased astrocyte swelling extent in response to hypoosmotic solution in brain slices (Fig 9), and discussed '... AQP4 can provide an efficient efflux pathway for water to leave astrocytes.' Correspondingly, our data suggest that AQP4 mediate astrocyte water efflux in basal conditions.

We have discussed the study (Igarashi et al., *NeuroReport* 2013); our current data would help to understand the cellular mechanisms underlying the finding of Igarashi et al.

The following is the authors' response to the original reviews.

**Public Reviews:**

**Reviewer #1 (Public Review):**

*Summary:*

*Pham and colleagues provide an illuminating investigation of aquaporin-4 water flux in the brain utilizing ex vivo and in vivo techniques. The authors first show in acute brain slices, and in vivo with fiber photometry, SRB-loaded astrocytes swell after inhibition of AQP4 with TGN-020, indicative of tonic water efflux from astrocytes in physiological conditions. Excitingly, they find that TGN-020 increases the ADC in DW-MRI in a region-specific manner, potentially due to AQP4 density. The resolution of the DW-MRI cannot distinguish between intracellular or extracellular compartments, but the data point to an overall accumulation of water in the brain with AQP4 inhibition. These results provide further clarity on water movement through AQP4 in health and disease.*

*Overall, the data support the main conclusions of the article, with some room for more detailed treatment of the data to extend the findings.*

*Strengths:*

*The authors have a thorough investigation of AQP4 inhibition in acute brain slices. The demonstration of tonic water efflux through AQP4 at baseline is novel and important in and of itself. Their further testing of TGN-020 in hyper- and hypo-osmotic solutions shows the expected reduction of swelling/shrinking with AQP4 blockade.*

*Their experiment with cortical spreading depression further highlights the importance of water efflux from astrocytes via AQP4 and transient water fluxes as a result of osmotic gradients. Inhibition of AQP4 increases the speed of tissue swelling, pointing to a role in the efflux of water from the brain.*

*The use of DW-MRI provides a non-invasive measure of water flux after TGN-020 treatment.*

We thank the reviewer for the insightful comments.

*Weaknesses:*

*The authors specifically use GCaMP6 and light sheet microscopy to image their brain sections in order to identify astrocytic microdomains. However, their presentation of the data neglects a more detailed treatment of the calcium signaling. It would be quite interesting to see whether these calcium events are differentially affected by AQP4 inhibition based on their cellular localization (ie. processes vs. soma vs. vascular end feet which all have different AQP4 expressions).*

Following the suggestion, we provide new data on the effect of AQP4 inhibition on spontaneous calcium signals in perivascular astrocyte end-feet. As shown now in Fig.S2, acute application of TGN020 induced Ca<sup>2+</sup> oscillations in astrocyte end-feet regions where the GCaMP6 labeling lines the profile of the blood vessel. It is noted that on average, the strength of basal Ca<sup>2+</sup> signals in the end-feet is higher than that observed across global astrocyte territories ( $4.65 \pm 0.55$  vs.  $1.45 \pm 0.79$ ,  $p < 0.01$ ), as does the effect of TGN ( $8.4 \pm 0.62$  vs.  $6.35 \pm 0.97$ ,  $p < 0.05$ ; Fig S2 vs. Fig 2B). This likely reflects the enrichment of AQP4 in astrocyte end-feet. We describe the data in Fig.S2, and on page 8, line 20 – 23.

We now use the transgenic line GLAST-GCaMP6 for cytosolic GCaMP6 expression in astrocytes. Spontaneous calcium signals, reflected by transient fluorescence rises, occur in discrete micro-domains whereas the basal GCaMP6 fluorescence in the soma is weak. In the present condition, it is difficult to unambiguously discriminate astrocyte soma from the highly intermingled processes.

*The authors show the inhibition of AQP4 with TGN-020 shortens the onset time of the swelling associated with cortical spreading depression in brain slices. However, they do not show quantification for many of the other features of CSD swelling, (ie. the duration of swelling, speed of swelling, recovery from swelling).*

Regarding the features of the CSD swelling, we have performed new analysis to quantify the duration of swelling, speed of swelling and the recovery time from swelling in control condition and in the presence of TGN-020. The new analysis is now summarized in Fig. S5. Blocking AQP4 with TGN-020 increases the swelling speed, prolongs the duration of swelling and slows down the recovery from swelling, confirming our observation that acute inhibition of AQP4 water efflux facilitates astrocyte swelling while restrains shrinking. We describe the result on page 11, line 19-21.

#### *Significance:*

*AQP4 is a bidirectional water channel that is constitutively open, thus water flux through it is always regulated by local osmotic gradients. Still, characterizing this water flux has been challenging, as the AQP4 channel is incredibly water-selective. The authors here present important data showing that the application of TGN-020 alone causes astrocytic swelling, indicating that there is constant efflux of water from astrocytes via AQP4 in basal conditions. This has been suggested before, as the authors rightfully highlight in their discussion, but the evidence had previously come from electron microscopy data from genetic knockout mice.*

*AQP4 expression has been linked with the glymphatic circulation of cerebrospinal fluid through perivascular spaces since its rediscovery in 2012 [1]. Further studies of aging[2], genetic models[3], and physiological circadian variation[4] have revealed it is not simply AQP4 expression but AQP4 polarization to astrocytic vascular endfeet that is imperative for facilitating glymphatic flow. Still, a lingering question in the field is how AQP4 facilitates fluid circulation. This study represents an important step in our understanding of AQP4's function, as the basal efflux of water via AQP4 might promote clearance of interstitial fluid to allow an influx of cerebrospinal fluid into the brain. Beyond glymphatic fluid circulation, clearly, AQP4-dependent volume changes will differentially alter astrocytic calcium signaling and, in turn, neuronal activity.*

*(1) Iliff, J.J., et al., A Paravascular Pathway Facilitates CSF Flow Through the Brain Parenchyma and the Clearance of Interstitial Solutes, Including Amyloid  $\beta$ . Sci Transl Med, 2012. 4(147): p. 147ra111.*

*(2) Kress, B.T., et al., Impairment of paravascular clearance pathways in the aging brain. Ann Neurol, 2014. 76(6): p. 845-61.*

*(3) Mestre, H., et al., Aquaporin-4-dependent Glymphatic Solute Transport in the Rodent Brain. eLife, 2018. 7.*

*(4) Hablitz, L., et al., Circadian control of brain glymphatic and lymphatic fluid flow. Nature Communications, 2020. 11(1).*

We thank the reviewer in acknowledging the significance of our study and the functional implication in brain glymphatic system. We have now highlighted the mentioned studies as well as the potential implication glymphatic fluid circulation (page 4, line 9-10; page 5, line 1-3; and page 19, line 3-10).

**Reviewer #2 (Public Review):**

*Summary:*

*The paper investigates the role of astrocyte-specific aquaporin-4 (AQP4) water channel in mediating water transport within the mouse brain and the impact of the channel on astrocyte and neuron signaling. Throughout various experiments including epifluorescence and light sheet microscopy in mouse brain slices, and fiber photometry or diffusion-weighted MRI in vivo, the researchers observe that acute inhibition of AQP4 leads to intracellular water accumulation and swelling in astrocytes. This swelling alters astrocyte calcium signaling and affects neighboring neuron populations. Furthermore, the study demonstrates that AQP4 regulates astrocyte volume, influencing mainly the dynamics of water efflux in response to osmotic challenges or associated with cortical spreading depolarization. The findings suggest that AQP4-mediated water efflux plays a crucial role in maintaining brain homeostasis, and indicates the main role of AQP4 in this mechanism. However authors highlight that the report sheds light on the mechanisms by which astrocyte aquaporin contributes to the water environment in the brain parenchyma, the mechanism underlying these effects remains unclear and not investigated. The manuscript requires revision.*

*Strengths:*

*The paper elucidates the role of the astrocytic aquaporin-4 (AQP4) channel in brain water transport, its impact on water homeostasis, and signaling in the brain parenchyma. In its idea, the paper follows a set of complimentary experiments combining various ex vivo and in vivo techniques from microscopy to magnetic resonance imaging. The research is valuable, confirms previous findings, and provides novel insights into the effect of acute blockage of the AQP4 channel using TGN-020.*

We thank the reviewer for the constructive comments.

*Weaknesses:*

*Despite the employed interdisciplinary approach, the quality of the manuscript provides doubts regarding the significance of the findings and hinders the novelty claimed by the authors. The paper lacks a comprehensive exploration or mention of the underlying molecular mechanisms driving the observed effects of astrocytic aquaporin-4 (AQP4) channel inhibition on brain water transport and brain signaling dynamics. The scientific background is not very well prepared in the introduction and discussion sections. The important or latest reports from the field are missing or incompletely cited and misconcluded. There are several citations to original works missing, which would clarify certain conclusions. This especially refers to the basis of the glymphatic system concept and recently published reports of similar content. The usage of TGN-020, instead of i.e. available AER-270(271) AQP4 blocker, is not explained. While employing various experimental techniques adds depth to the findings, some reasoning behind the employed techniques - especially regarding MRI - is not clear or seemingly inaccurate. Most of the time the number of subjects examined is lacking or mentioned only roughly within the figure captions, and there are lacking or wrongly applied statistical tests, that limit assessment and reproducibility of the results. In some cases, it seems that two different statistical tests were used for the same or linked type of data, so the results are*

*contradictory even though appear as not likely - based on the figures. Addressing these limitations could strengthen the paper's impact and utility within the field of neuroscience, however, it also seems that supplementary experiments are required to improve the report.*

The current data hint at a tonic water efflux from astrocyte AQP4 in physiological condition, which helps to understand brain water homeostasis and the functional implication for the glymphatic system. The underlying molecular and cellular mechanisms appear multifaceted and functionally interconnected, as discussed (page 14 line 8 –page 15, line 3). We agree that a comprehensive exploration will further advance our understanding.

The introduction and discussion are now strengthened by incorporating the important advances in glymphatic system while highlighting the relevant studies.

The use of TGN-020 was based on its validation by wide range of ex vivo and in vivo studies including the use of heterologous expression system and the AQP4 KO mice. The validation of AER-270(271, the water soluble prodrug) using AQP4 KO mice is reported recently (Giannetto et al., 2024). AER-271 was noted to impact brain water ADC (apparent diffusion coefficient evaluated by diffusion-weighted MRI) in AQP4 KO mice ~75 min after the drug application (Giannetto et al., 2024). This likely reflects that AER270(271) is also an inhibitor for  $\kappa$ B nuclear factor (NF- $\kappa$ B) whose inhibition could reduce CNS water content independent of AQP4 targeting (Salman et al., 2022). In addition, the inhibition efficiency of AER-270(271) seems lower than TGN-020 (Farr et al., 2019; Giannetto et al., 2024; Huber et al., 2009; Salman et al., 2022). We have now supplemented this information in the manuscript (page 7, line 1-6 and page15, line 7-17).

The description on the DW-MRI is now updated (page 4, line 10-14).

We also performed new experiments and data analysis as described in a point-to-point manner below in the section 'Recommendations For The Authors'.

#### **Reviewer #3 (Public Review):**

##### *Summary:*

*In this manuscript, the authors propose that astrocytic water channel AQP4 represents the dominant pathway for tonic water efflux without which astrocytes undergo cell swelling. The authors measure changes in astrocytic sulforhodamine fluorescence as the proxy for cell volume dynamics. Using this approach, they perform a technically elegant series of ex vivo and in vivo experiments exploring changes in astrocytic volume in response to AQP4 inhibitor TGN-020 and/or neuronal stimulation. The key finding is that TGN-020 produces an apparent swelling of astrocytes and modifies astrocytic cell volume regulation after spreading depolarizations. Additionally, systemic application of TGN-020 produced changes in diffusion-weighted MRI signal, which the authors interpret as cellular swelling. This study is perceived as potentially significant. However, several technical caveats should be strongly considered and perhaps addressed through additional experiments.*

##### *Strengths:*

*(1) This is a technically elegant study, in which the authors employed a number of complementary ex vivo and in vivo techniques to explore functional outcomes of aquaporin inhibition. The presented data are potentially highly significant (but see below for caveats and questions related to data interpretation).*

*(2) The authors go beyond measuring cell volume homeostasis and probe for the functional significance of AQP4 inhibition by monitoring  $\text{Ca}^{2+}$  signaling in neurons and*

*astrocytes (GCaMP6 assay).*

*(3) Spreading depolarizations represent a physiologically relevant model of cellular swelling. The authors use ChR2 optogenetics to trigger spreading depolarizations. This is a highly appropriate and much-appreciated approach.*

We thank the reviewer for the effort in evaluating our work.

*Weaknesses:*

*(1) The main weakness of this study is that all major conclusions are based on the use of one pharmacological compound. In the opinion of this reviewer, the effects of TGN-020 are not consistent with the current knowledge on water permeability in astrocytes and the relative contribution of AQP4 to this process.*

*Specifically: Genetic deletion of AQP4 in astrocytes reduces plasmalemmal water permeability by ~two-three-fold (when measured at 37°C, Solenov et al., AJP-Cell, 2004). This is a significant difference, but it is thought to have limited/no impact on water distribution. Astrocytic volume and the degree of anisotonic swelling/shrinkage are unchanged because the water permeability of the AQP4null astrocytes remains high. This has been discussed at length in many publications (e.g., MacAulay et al., Neuroscience, 2004; MacAulay, Nat Rev Neurosci, 2021) and is acknowledged by Solenov and Verkman (2004).*

*Keeping this limitation in mind, it is important to validate astrocytic cell volume changes using an independent method of cell volume reconstruction (diameter of sulforhodamine-labeled cell bodies? 3D reconstruction of EGFP-tagged cells? Else?)*

Solenov and coll. used the calcein quenching assay and KO mice demonstrating AQP4 as a functional water channel in cultured astrocytes (Solenov et al., 2004). AQP4 deletion reduced both astrocyte water permeability and the absolute amplitude of swelling over comparable time, and also slowed down cell shrinking, which overall parallels our results from acute AQP4 blocking. Yet in Solenov's study, the time to swelling plateau was prolonged in AQP4 KO astrocytes, differing from our data from the pharmacological acute blocking. This discrepancy may be due to compensatory mechanisms in chronic AQP4 KO, or reflect the different volume responses in cultured astrocytes from brain slices or in vivo results as suggested previously (Risher et al., 2009).

Soma diameter might be an indicator of cell volume change, yet it is challenging with our current fluorescence imaging method that is diffraction-limited and insufficient to clearly resolve the border of the soma *in situ*. In addition, the lateral diameter of cell bodies may not faithfully reflect the volume changes that can occur in all three dimensions. Rapid 3D imaging of astrocyte volume dynamics with sufficient high Z-axis resolution appears difficult with our present tools.

We have now accordingly updated the discussion with relevant literatures being cited (page 17 line 14 – page 18, line 3).

*(2) TGN-020 produces many effects on the brain, with some but not all of the observed phenomena sensitive to the genetic deletion of AQP4. In the context of this work, it is important to note that TGN020 does not completely inhibit AQP4 (70% maximal inhibition in the original oocyte study by Huber et al., Bioorg Med Chem, 2009). Thus, besides not knowing TGN-020 levels inside the brain, even*

*"maximal" AQP4 inhibition would not be expected to dramatically affect water permeability in astrocytes.*

*This caveat may be addressed through experiments using local delivery of structurally unrelated AQP4 blockers, or, preferably, AQP4 KO mice.*

It is an important point that TGN-020 partially blocks AQP4, implying the actual functional impact of AQP4 per se might be stronger than what we observed. TGN provides a means to acutely probe AQP4 function *in situ*, still we agree, its limitation needs be acknowledged. We mention this now on page 15, line 7-9 and 14-17.

We agree that local delivery of an alternative blocker will provide additional information. Meanwhile, local delivery requires the stereotaxic implantation of cannula, which would cause inflammations to surrounding astrocytes (and neurons). The recently introduced AQP4 blocker AER-270(271) has received attention that it influences brain water dynamics (ADC in DW-MRI) in AQP4 KO mice (Giannetto et al., 2024), recalling that AER-270(271) is also an inhibitor for  $\kappa$ B nuclear factor (NF- $\kappa$ B). This pathway can potentially perturb CNS water content and influence brain fluid circulation, in an AQP4-independent manner (Salman et al., 2022). The inhibition efficiency on mouse AQP4 of AER-270 (~20%, Farr et al., 2019; Salman et al., 2022) appears lower than TGN-020 (~70%, Huber et al., 2009).

We chose to use the pharmacological compound to achieve acute blocking of AQP4 thereby avoiding the chronic genetics-caused alterations in brain structural, functional and water homeostasis. Multiple lines of evidence including the recent study (Gomolka et al., 2023), have shown that AQP4 KO mice alters brain water content, extracellular space and cellular structures, which raises concerns to use the transgenic mouse to pinpoint the physiological functions of the AQP4 water channel.

We have now mentioned the concerns on AQP4 pharmacology by supplementing additional literatures in the field (page 15, line 8-18).

*(3) This reviewer thinks that the ADC signal changes in Figure 5 may be unrelated to cellular swelling. Instead, they may be a result of the previously reported TGN-020-induced hyphemia (e.g., H. Igarashi et al., NeuroReport, 2013) and/or changes in water fluxes across pia matter which is highly enriched in AQP4. To amplify this concern, AQP4 KO brains have increased water mobility due to enlarged interstitial spaces, rather than swollen astrocytes (RS Gomolka, eLife, 2023). Overall, the caveats of interpreting DW-MRI signal deserve strong consideration.*

The previous observation show that TGN-020 increases regional cerebral blood flow in wild-type mice but not in AQP4 KO mice (Igarashi et al., 2013). Our current data provide a possible mechanism explanation that TGN-020 blocking of astrocyte AQP4 causes calcium rises that may lead to vasodilation as suggested previously (Cauli and Hamel, 2018). We now add updates to the discussion on page 15, line 3-7.

We are in line with the reviewer regarding the structural deviations observed with the AQP4 KO mice

(Gomolka et al., 2023), now mentioned on page 19, line 3-5. Following the Reviewer's suggestion, we have also updated the interpretation of the DW-MRI signal and point that in addition to being related to the astrocyte swelling, the ADC signal changes may also be caused by indirect mechanisms, such as the transient upregulation of other water-permeable pathways in compensating AQP4 blocking. We now describe this alternative interpretation and the caveats of the DW-MRI signals (page 20, line 1-8).

**Recommendations for the authors:**

## **Reviewer #1 (Recommendations For The Authors):**

### *Private recommendations*

*My more broad experimental suggestions are in the "weaknesses" section. Some minor points that would improve the manuscript are included below:*

*(1) A more detailed explanation for why SRB fluorescence reflects the astrocyte volume changes, whereas typical intracellular GFP does not.*

As an engineered fluorescence protein, the GFP has been used to tag specific type of cells. Meanwhile, as a relatively big protein (MW, 26.9 kDa), the diffusion rate of EGFP is expected to be much less than SRB, a small chemical dye (MW, 558.7 Da). Also, the IP injection of SRB enables geneticsless labeling of brain astrocytes, so to avoid the influence of protein overexpression on astrocyte volume and water transport responses. We have now stated this point in the manuscript (page 13, line 21 – page 14, line 4).

*(2) Figure 1 panel B should have clear labels on the figure and a description in the legend to delineate which part of the panel refers to hyper- or hypo-osmotic treatment.*

We have now updated the figure and the legend.

*(3) For Figure 2, what is the rationale for analyzing the calcium signaling data between the cell types differently?*

We analyzed calcium micro-domains for astrocytes as their spontaneous signals occur mainly in discrete micro-domains (Shigetomi et al., 2013). While for neurons, we performed global analysis by calculating the mean fluorescence of imaging field of view, because calcium signal changes were only observed at global level rather than in micro-domains. This information is now included (page 24, line 1820).

*(4) For Figure 3, the authors mention that TGN-020 likely caused swelling prior to the hypotonic solution administration. Do they have any measurements from these experiments prior to the TGN-020 application to use as a "true baseline" volume?*

The current method detects the relative changes in astrocyte volume (i.e., transmembrane water transport), which nevertheless is blind to the absolute volume value. We have no readout on baseline volumes.

*(5) For Figures 3 and 4, did the authors see any evidence for regulatory volume decrease? And is this impaired by TGN-020? It is a well-characterized phenomenon that astrocytes will open mechanosensitive channels to extrude ions during hypo-osmotic induced swelling. This process is dependent on AQP4 and calcium signaling [5]*

Mola and coll. provided important results demonstrating the role of AQP4 in astrocyte volume regulation (Mola et al., 2016). In the present study in acute brain slices, when we applied hypotonic solution to induce astrocyte swelling, our protocol did not reveal rapid regulatory volume decrease (e.g., Fig. 3D). When we followed the volume changes of SRB-labeled astrocytes during optogenetically induced CSD, we observed the phase of volume decrease following the transient swelling (Fig. 4F), where the peak amplitude and the degree of recovery were both reduced by inhibiting AQP4 with TGN020. These data imply that regulatory astrocyte volume decrease may occur in specific conditions, which intriguingly has been suggested to be absent in brain slices and in vivo (e.g., Risher et al., 2009). We have

not specifically investigated this phenomenon, and now briefly discuss this point on page18 line 6-14.

(6) Figure 5 box plots do not show all data points, could the authors modify to make these plots show all the animals, or edit the legend to clarify what is plotted?

We have now updated the plot and the legend. This plot is from all animals (n = 7 per condition).

(7) pg. 9 line 6, there is a sentence that seems incomplete or otherwise unfinished. "We first followed the evoked water efflux and shrinking induced by hypertonic solution while."

Fixed (now, page 9 line 17-18).

(8) During the discussion on pg 13 line 11, it may be more clear to describe this as the cotransport of water into the cells with ions/metabolites as reviewed by Macaulay 2021 [6].

We agree; the text is modified following this suggestion (now page14, line 12-13).

(1) Iliff, J.J., et al., A Paravascular Pathway Facilitates CSF Flow Through the Brain Parenchyma and the Clearance of Interstitial Solutes, Including Amyloid  $\beta$ . *Sci Transl Med*, 2012. 4(147): p. 147ra111.

(2) Kress, B.T., et al., Impairment of paravascular clearance pathways in the aging brain. *Ann Neurol*, 2014. 76(6): p. 845-61.

(3) Mestre, H., et al., Aquaporin-4-dependent Glymphatic Solute Transport in the Rodent Brain. *eLife*, 2018. 7.

(4) Hablitz, L., et al., Circadian control of brain glymphatic and lymphatic fluid flow. *Nature Communications*, 2020. 11(1).

(5) Mola, M., et al., The speed of swelling kinetics modulates cell volume regulation and calcium signaling in astrocytes: A different point of view on the role of aquaporins. *Glia*, 2016. 64(1).

(6) MacAulay, N., Molecular mechanisms of brain water transport. *Nat Rev Neurosci*, 2021. 22(6): p. 326-344.

We thank the reviewer. These important literatures are now supplemented to the manuscript together with the corresponding revisions.

#### **Reviewer #2 (Recommendations For The Authors):**

*In its concept, the paper is interesting and provides additional value - however, it requires revision.*

*Below, I provide the following remarks for the following sections/ pages/lines:*

*ABSTRACT/page 2 (remarks here refer to the rest of the manuscript, where these sentences are repeated):*

*- It seems that the 'homeostasis' provides not only physical protection, but also determines the diffusion of chemical molecules...' Please correct the sentence as it is grammatically incorrect.*

It is now corrected (page 2, line 1).

- *The term 'tonic water' is not clear. I understand, after reading the paper, that it is about tonicity of the solutes injected into the mouse.*

We use the term 'tonic' to indicate that in basal conditions, a constant water efflux occurs through the AQP4 channel.

- *'tonic aquaporin water efflux maintains volume equilibrium' - I believe it is about maintaining volume and osmotic equilibrium?*

This description is now refined (now page 2, line 10).

- *It is not clear whether the tonic water outflow refers to the cellular level or outflow from the brain parenchyma (i.e., glymphatic efflux)*

It refers to the cellular level.

INTRODUCTION/page 3:

- *'clearance of waste molecules from the brain as described in the glymphatic system' - The original papers describing the phenomena are not cited: Iliff et al. 2012, 2013, Mestre et al. 2018, as well as reviews by Nedergaard et al.*

Indeed. We have now cited these key literatures (now page 4, line 10).

- *'brain water diffusion is the basis for diffusion-weighted magnetic resonance imaging (DW-MRI)' - The statement is wrong. it is the mobility of the water protons that DWI is based on, but not the diffusion of molecules in the brain. This should be clarified and based on the DW-MRI principle and the original works by Le Bihan from 1986, 1988, or 2015.*

This sentence is now updated (page 4, line10-14).

- *Similarly, I suggest correcting or removing the citations and the sentence part regarding the clinical use of DWI, as it has no value here. Instead, it would be worth mentioning what actually ADC reflects as a computational score, and what were the results from previous studies assessing glymphatic systems using DWI. This is especially important when considering the mislocalization of the AQP4 channel.*

We now states recent studies using DW-MRI to evaluate glymphatic systems (page 4, line16-17).

- *'In the brain, AQP4 is predominantly expressed in astrocytes'-please review the citations. I suggest reading the work by Nielsen 1997, Nagelhus 2013, Wolburg 2011, and Li and Wang from 2017. To my best knowledge, in the brain AQP4 is exclusively expressed in astrocytes.*

Thanks for the reviewer. It is described that while enriched in astrocytes, AQP4 is also expressed in ependymal cells lining the ventricles (e.g., (Mayo et al., 2023; Verkman et al., 2006)). 'predominantly' is now removed (page 4, line 21).

- *The conclusion: ' Our finding suggests that aquaporin acts as a water export route in astrocytes in physiological conditions, so as to counterbalance the constitutive*

*intracellular water accumulation caused by constant transmitter and ion uptake, as well as the cytoplasmic metabolism processes. This mechanism hence plays a necessary role in maintaining water equilibrium in astrocytes, thereby brain water homeostasis' seems to be slightly beyond the actual findings in the paper. I suggest clarifying according to the described phenomena.*

We have now refined the conclusion sticking to the experimental observations (page 5, line16-18).

*- The introduction lacks important information on existing AQP4 blockers and their effects, pros and cons on why to use TGN-020. Among others, I would refer to recent work by Giannetto et al 2024, as well as previous work of Mestre et al. 2018 and Gomolka et al. 2023.*

We initiated the study by using TGN-020 as an AQP4 blocker because it has been validated by wide range of ex vivo and in vivo studies as documented in the text (page 7, line 1-6). We also update discussions on the recent advances in validating the AQP4 blocker AER-270(271) while citing the relevant studies (page 15, line 7-17).

#### RESULTS:

*- Page 5, lines 19-20: '...transport, we performed fluorescence intensity translated (FIT) imaging.' - this term was never introduced in the methods so it is difficult for the reader to understand it at first sight. -'To this end,' - it is not clear which action refers to 'this'. (is it about previous works or the moment that the brain samples were ready for imaging? Please clarify, as it is only starting to be clear after fully reading the methods.*

We now refine the description give the principle of our imaging method first, then explain the technical steps. To avoid ambiguity, the term ‘To this end’ is removed. The updated text is now on page 6, line 1-3.

*- From page 6 onwards - all references to Figures lack information to which part of the figure subpanel the information refers (top/middle bottom or left/middle/right).*

We apologize. The complementary indication is now added for figure citations when applicable.

*- 'whereas water export and astrocyte shrinking upon hyperosmotic manipulation increased astrocyte fluorescence (Figure 1B). Hence, FIT imaging enables real-time recording of astrocyte transmembrane water transport and volume dynamics.' - this part seems to be undescribed or not clear in the methods.*

We have now refined this description (page 6, line 19-20).

*- Page 6, lines 17-22: TGN-020. In addition to the above, I suggest familiarizing also with the following works by Igarashi 2011. doi: 10.1007/s10072-010-0431-1, and by Sun 2022. doi: 10.3389/fimmu.2022.870029.*

These studies are now cited (page 7, line 3-4).

*- Page 7: ' AQP4 is a bidirectional channel facilitating... ' - AQP4 water channel is known as the path of least resistance for water transfer, please see Manley, Nature Medicine, 2000 and Papadopoulos, Faseb J, 2004.*

This sentence is now updated (page 7, line 12-13).

*- ' astrocyte AQP4 by TGN-020 caused a gradual decrease in SRB fluorescence intensity, indicating an intracellular water accumulation' - tissue slice experiment is a very valuable method. However it seems right, the experiment does not comment on the cell swelling that may occur just due to or as a superposition of tissue deterioration and the effect of TGN-020. The AQP4 channel is blocked, and the influx of water into astrocytes should be also blocked. Thus, can swelling be also a part of another mechanism, as it was also observed in the control group? I suggest this should be addressed thoroughly.*

We performed this experiment in acute brain slices to well control the pharmacological environment and gain spatial-temporal information. Post slicing, the brain slices recovered > 1hr prior to recording, so that the slices were in a stable state before TGN-020 application as evidenced by the stable baseline. The constant decrease in the control trace is due to photobleaching which did not change its curve tendency in response to vehicle. TGN-020, in contrast, caused a down-ward change suggesting intracellular water accumulation and swelling.

The experiment was performed at basal condition without active water influx; a decrease in SRB fluorescence hints astrocyteintracellular water buildup. This result shows that in basal condition, astrocyte aquaporin mediates a constant (i.e., tonic) water efflux; its blocking causes intracellular water accumulation and swelling.

We have accordingly updated the description of this part (page 7, line 15-20).

*- From the Figure 1 legend: Only 4 mice were subjected to the experiment, and only 1 mouse as a control. I suggest expanding the experiment and performing statistics including two-way ANOVA for data in panels B, C, and D, as no results of statistical tests confirm the significance of the findings provided.*

The panel B confirms that cytosolic SRB fluorescence displays increasing tendency upon water efflux and volume shrinking, and vice versa. As for the panel C, the number of mice is now indicated. Also, the downward change in the SRB fluorescence was now respectively calculated for the phases prior and post to TGN (and vehicle) application, and this panel is accordingly updated. TGN-020 induced a declining in astrocyte SRB fluorescence, which is validated by t-test performed in MATLAB. To clarify, we now add cross-link lines to indicate statistical significance between the corresponding groups (Fig 1C, middle). As for panel D, we calculated the SRB fluorescence change (decrease) relative to the photobleaching tendency illustrated by the dotted line. The significance was also validated by t-test performed in MATLAB.

*- Figure 1: Please correct the figure - pictures in panel A are low quality and do not support the specificity of SRB for astrocytes. Panels B-D are easier to understand if plotted as normal X/Y charts with associated statistical findings. Some drawings are cut or not aligned.*

In GFAP-EGFP transgenic, astrocytes are labeled by EGFP. SRB labeling (red fluorescence) shows colocalization with EGFP-positive astrocytes, meanwhile not all EGFP-positive astrocytes are labeled by SRB. The PDF conversion procedure during the submission may also somehow have compromised image quality. We have tried to update and align the figure panels.

*- Page 12: ' TGN-020 increased basal water diffusion within multiple regions including the cortex,*

hippocampus and the striatum in a heterogeneous manner (Figure 5C).'

This sentence is updated now (page 12, line 12 – page13, line 2). It reads 'The representative images reveal the enough image quality to calculate the ADC, which allow us to examine the effect of TGN-020 on water diffusion rate in multiple regions (Fig. 5C).'

*- The expression of AQP4 within the brain parenchyma is known to be heterogenous. Please familiarize yourself with works by Hubbard 2015, Mestre 2018, and Gomolka 2023. A correlation between ADC score and AQP4 expression ROI-wise would be useful, but it is not substantial to conduct this experiment.*

We thank the reviewer. This point is stressed on page 19, line 12-14.

#### DISCUSSION:

*- Most of the issues are commented on above, so I suggest following the changes applied earlier. -Page 16: 'We show by DW-MRI that water transport by astrocyte aquaporin is critical for brain water homeostasis.' This statement is not clear and does not refer to the actual impact of the findings. DWI is allowed only to verify the changes of ADC fter the application of TGN-020. I suggest commenting on the recent report by Giannetto 2024 here.*

This sentence is now refined (page 19, line 1-2), followed by the updates commenting on the recent studies employing DW-MRI to evaluate brain fluid transport, including the work of (Giannetto et al., 2024) (page 19, line 3-10).

#### METHODS:

*- Page 18: no total number of mice included in all experiments is provided, as well as no clearly stated number of mice used in each experiment. Please correct.*

We have now double checked the number of the mice for the data presented and updated the figure legends accordingly (e.g., updates in legends fig1, fig5, etc).

- Page 18, line 7: 'Axscience' is not a producer of Isoflurane, but a company offering help with scientific manuscript writing. If this company's help was used, it should be stated in the acknowledgments section. Reference to ISOVET should be moved from line 15 to line 7.

We apologize. We did not use external writing help, and now have removed the 'Axcience'. The Isoflurane was under the mark 'ISOVET' from 'Piramal'. This info is now moved up (page 21, line 11).

*- Page 18, line 9: ' modified artificial cerebrospinal fluid (aCSF)'. Additional information on the reason for the modified aCSF would be useful for the reader.*

In this modified solution, the concentration of depolarizing ions (Na<sup>+</sup>, Ca<sup>2+</sup>) was reduced to lower the potential excitotoxicity during the tissue dissection (i.e., injury to the brain) for preparing the brain slices. Extra sucrose was added to balance the solution osmolarity. This solution has been used previously for the dissection and the slicing steps in adult mice (Jiang et al., 2016). We now add this justification in the text and quote the relevant reference (page 21, line14-16).

*- Page 19, line 6: a reasoning for using Tamoxifen would be helpful for the reader.*

The Glast-CreERT2 is an inducible conditional mouse line that expresses Cre recombinase selectively in astrocytes upon tamoxifen injection. We now add this information in the text (page 22, line 10-11).

| - Line 8 - 'Sigma'

Fixed.

| - Line 7/8: It is not clear if ethanol is of 10% solution or if proportions of ethanol+tamoxifen to oil were of 1:9. The reasoning for each performed step is missing.

We have now clarified the procedure (page 22, line 11-15).

| - Line 10: '/' means 'or'?

Here, we mean the bigenic mice resulting from the crossing of the heterozygous Cre-dependent GCaMP6f and Glast-CreERT2 mouse lines. We now modify it to 'Glast-CreERT2::Ai95GCaMP6f//WT', in consistence with the presentation of other mouse lines in our manuscript (page 22, line 16).

| - Lines 22-23: being in-line with legislation was already stated at the beginning of the Methods so I suggest combining for clearance.

Done.

| - Page 21, line 4: it is good to mention which printer was used, but it would be worth mentioning the material the chamber was printed from - was it ABS?

Yes. We add this info in the text now (page 24, line 5).

| - Line 9 - 'PI' requires spelling out.

It is 'Physik Instrumente', now added (page 24, line 10).

| - Line 11-12: What is the reason for background subtraction - clearer delineation of astrocytes/ increasing SNR in post-processing, or because SRB signal was also visible and changing in the background over time? Was the background removed in each frame independently (how many frames)? How long was the time-lapse and was the F0 frame considered as the first frame acquired? The background signal should be also measured and plotted alongside the astrocytic signal, as a reference (Figure 1). This should be clarified so that steps are to be followed easily.

We sought to follow the temporal changes in SRB fluorescence signal. The acquired fluorescent images contain not only the SRB signals, but also the background signals consisting of for instance the biological tissue autofluorescence, digital camera background noise and the leak light sources from the environments. The value of the background signal was estimated by the mean fluorescence of peripheral cell-free subregions ( $15 \times 15 \mu\text{m}^2$ ) and removed from all frames of time-lapse image stack. The traces shown in the figures reflect the full lengths of the time-lapse recordings. F0 was identified as the mean value of the 10 data points immediately preceding the detected fluorescence changes. The text is now updated (page 24 line 21 - page 25 line 5).

- Line 15: Was astrocyte image delineation performed manually or automatically? Where was the center of the region considered in the reference to the astrocyte image? It would be good to see the regions delineated for reference.

Astrocytes labeled by SRB were delineated manually with the soma taken as the center of the region of interest. We now exemplify the delineated region in Fig 1A, bottom.

- Page 22, line 2: 'x4 objective'.

Added (now, page 25, line 16).

- Line 3: 'barrels' - reference to publication or the explanation missing.

The relevant reference is now added on barrel cortex (Erzurumlu and Gaspar, 2020) (page 25, line 19-20).

- Line 19: were the coordinates referred to = bregma?

Yes. This info is now added (page 26, line 12).

- Line 20: was the habituation performed directly at the acquisition date? It is rather difficult to say that it was a habituation, but rather acute imaging. I suggest correcting, that mice were allowed to familiarize themselves with the setup for 30 minutes prior to the imaging start.

*In this context, although it is a very nice idea and experiment, the influence of acute stress in animals familiar with the setup only from the day of acquisition is difficult to avoid. It is a major concern, especially when considering norepinephrine as a master driver of neuronal and vascular activity through the brain, and strong activation of the hypothalamic-adrenal axis in response to acute stress. It is well known, that the response of monoamines is reduced in animals subjected to chronic v.s acute stress, but still larger than that if the stressor is absent.*

*Major remark: The animals should, preferably, be imaged at least after 3 days of habituation based on existing knowledge. I suggest exploring the topic of the importance of habituation. It is difficult though, to objectively review these findings without considering stress and associated changes in vascular dynamics.*

Many thanks for the reviewer to help to precise this information. The text is accordingly updated to describe the experiment (now page 26, line 14).

- Page 23, line 17: number of animals included in experiments missing.

The number of animals is added in Methods (page 27, line 12) and indicated in the legend of Figure 5.

- Line 18/19: were the respiratory effects observed after injection of saline or TGN-020? Since DWI was performed, the exclusion of perfusive flow on ADC is impossible.

*I suggest an additional experiment in n=3 animals per group, verifying the HR (and if possible BP) response after injection of TGN-020 and saline in mice.*

The respiratory rate has been recorded. We added the averaged respiratory rate before and after injection of TGN-020 or saline (now, Fig. S6; page 13, line 5-6).

- Line 22: Please, provide the model of the scanner, the model of the cryoprobe, as well as the model of the gradient coil used, otherwise it is difficult to assess or repeat these experiments.

We have now added the information of MRI system in Methods section (page 27, line17-21).

- Page 24: line 3/4: although the achieved spatial resolution of DWI was good and slightly lower than desired and achievable due to limitations of the method itself as well as cryoprobe, it is acceptable for EPI in mice.

Still, there is no direct explanation provided on the reasoning for using surface instead of volumetric coil, as well as on assuming an anisotropic environment (6 diffusion directions) for DWI measurements. This is especially doubtful if such a long echo-time was used alongside lower-thanpossible spatial resolution. Longer echo time would lower the SNR of the depicted signal but also would favor the depiction of signal from slow-moving protons and larger water pools. On the other hand, only 3 b-values were used, which is the minimum for ADC measurements, while a good research protocol could encompass at least 5 to increase the accuracy of ADC estimation and avoid undersampling between 250 and 1800 b-values. What was the reason for choosing this particular set of b-values and not 50, 600, and 2000? Besides, gradient duration time was optimally chosen, however, I have concerns about the decision for such a long gradient separation times.

If the protocol could have been better optimized, the assessment could have been also performed in respiratory-gated mode, allowing minimization of the effects of one of the lymphatic system driving forces.

Thus, I suggest commenting on these issues.

We chose the cryoprobe to increase the signal-to-noise ratio (SNR) in DW-MRI with long echo-time and high b-value. The volume coil has a more homogeneous SNR in the whole brain rather than the cryoprobe, but SNR should be reduced compared with cryoprobe. We confirmed that, even at the ventral part of the brain, the image quality of DW-MRI images was enough to investigate the ADC with cryoprobe (Fig. 5B-C). This is mentioned now in Methods (page 27, line 17-21).

We performed DW-MRI scanning for 5 min at each time-point using the condition of anisotropic resolution and 3 b-values, to investigate the time-course of ADC change following the injection of TGN020. Because the effect of TGN-020 appears about dozen of minutes post the injection (Igarashi et al., 2011), fast DW-MRI scanning is required. If isotropic DW-MRI with lower echo-time and more direction is used, longer scan time at each time point is required, maybe more than 1h. We agree that three bvalues is minimum to calculate the ADC and more b-values help to increase the accuracy. However, to achieve the temporal resolution so as to better catch the change of water diffusion, we have decided to use the minimum b-values. The previous study also validates the enough accuracy of DW-MRI with three b-values (Ashoor et al., 2019). Furthermore, previous study that used long diffusion time (> 20 ms) and long echo time (40 ms) shows the good mean diffusivity (Aggarwal et al., 2020), supporting that our protocol is enough to investigate the ADC. We have now updated the description (page 28 line 5-9). The reason why we choose the  $b = 250$  and  $1800 \text{ s/mm}^2$  is that  $2000 \text{ s/mm}^2$  seems too high to get the good quality of image. In the previous study, we have optimized that ADC is measurable with  $b = 0, 250, \text{ and } 1800 \text{ s/mm}^2$  (Debacker et al., 2020).

- Page 24, line 7: What was the post-processing applied for images acquired over 70 minutes? Did it consider motion-correction, co-registration, or drift-correction crucial to

*avoid pitfalls and mismatches in concluding data?*

The motion correction and co-registration were explained in Methods (page 28, line 12-14).

*Also, were these trace-weighted images or magnitude images acquired since DTI software was used for processing - while ADC fitting could be reliably done in Matlab, Python, or other software. Thus, was DSI software considering all 3 b-values or just used 0 and 1800 for the calculation of mean diffusivity for tractography (as ADC). The details should be explained.*

DSIstudio was used with all three b values ( $b = 0, 250, \text{ and } 1800 \text{ s/mm}^2$ ) to calculate the ADC. We added the description in Methods (page 28, line 16-18).

*To make sure that the results are not affected by the MR hardware, I suggest performing 3 control measurements in a standard water phantom, and presenting the results alongside the main findings.*

Thanks for this suggestion. We have performed new experiments and now added the control measurement with three phantoms, that is water, undecane, and dodecane. These new data are summarized now in Fig. S7, showing the stability of ADC throughout the 70 min scanning. We have updated the description on Method part (page 28, line 9-11) and on the Results (page 13, line 6-8).

*- Line 13: were the ROI defined manually or just depicted from previously co-registered Allen Brain atlas?*

The ROIs of the cortex, the hippocampus, and the striatum were depicted with reference to Allen mouse brain atlas (<https://scalablebrainatlas.incf.org/mouse/ABA12>). This is explained in Methods (page 28, line 14-16).

*- Line 10: why the average from 1st and 2nd ADC was not considered, since it would reduce the influence of noise on the estimation of baseline ADC?*

We are sorry that it was a typo. The baseline was the average between 1st and 2nd ADC. We corrected the description (page 28, line 20).

**STATISTIC:**

*Which type of t-test - paired/unpaired/two samples was used and why? Mann-Whitney U-tets are used as a substitution for parametric t-tests when the data are either non-parametric or assuming normal distribution is not possible. In which case Bonferroni's-Holm correction was used? - I couldn't find any mention of any multiple-group analysis followed by multiple comparisons. Each section of the manuscript should have a description of how the quantitative data were treated and in which aim. I suggest carefully correcting all figures accordingly, and following the remarks given to the Figure 1.*

We used unpaired t-test for data obtained from samples of different conditions. Indeed, MannWhitney U-test is used when the data are non-parametric deviating from normal distributions. Bonferroni-Holm correction was used for multiple comparisons (e.g., Fig. 4D-E).

**Reviewer #3 (Recommendations For The Authors):**

*I think that the following statement is insufficient: "The authors commit to share data, documentation, and code used in analysis". My understanding is eLife expects that all key*

| *data to be provided in a supplement.*

We thank the reviewer; we follow the publication guidelines of eLife.

## References

- Aggarwal, M., Smith, M.D., and Calabresi, P.A. (2020). Diffusion-time dependence of diffusional kurtosis in the mouse brain. *Magn Reson Med* 84, 1564-1578.
- Ashoor, M., Khorshidi, A., and Sarkhosh, L. (2019). Estimation of microvascular capillary physical parameters using MRI assuming a pseudo liquid drop as model of fluid exchange on the cellular level. *Rep Pract Oncol Radiother* 24, 3-11.
- Cauli, B., and Hamel, E. (2018). Brain Perfusion and Astrocytes. *Trends in neurosciences* 41, 409-413.
- Debacker, C., Djemai, B., Ciobanu, L., Tsurugizawa, T., and Le Bihan, D. (2020). Diffusion MRI reveals in vivo and non-invasively changes in astrocyte function induced by an aquaporin-4 inhibitor. *PLoS One* 15, e0229702.
- Erzurumlu, R.S., and Gaspar, P. (2020). How the Barrel Cortex Became a Working Model for Developmental Plasticity: A Historical Perspective. *J Neurosci* 40, 6460-6473.
- Farr, G.W., Hall, C.H., Farr, S.M., Wade, R., Detzel, J.M., Adams, A.G., Buch, J.M., Beahm, D.L., Flask, C.A., Xu, K., et al. (2019). Functionalized Phenylbenzamides Inhibit Aquaporin-4 Reducing Cerebral Edema and Improving Outcome in Two Models of CNS Injury. *Neuroscience* 404, 484-498.
- Giannetto, M.J., Gomolka, R.S., Gahn-Martinez, D., Newbold, E.J., Bork, P.A.R., Chang, E., Gresser, M., Thompson, T., Mori, Y., and Nedergaard, M. (2024). Glymphatic fluid transport is suppressed by the aquaporin-4 inhibitor AER-271. *Glia*.
- Gomolka, R.S., Hablitz, L.M., Mestre, H., Giannetto, M., Du, T., Hauglund, N.L., Xie, L., Peng, W., Martinez, P.M., Nedergaard, M., et al. (2023). Loss of aquaporin-4 results in glymphatic system dysfunction via brain-wide interstitial fluid stagnation. *eLife* 12.
- Huber, V.J., Tsujita, M., and Nakada, T. (2009). Identification of aquaporin 4 inhibitors using in vitro and in silico methods. *Bioorg Med Chem* 17, 411-417.
- Igarashi, H., Huber, V.J., Tsujita, M., and Nakada, T. (2011). Pretreatment with a novel aquaporin 4 inhibitor, TGN-020, significantly reduces ischemic cerebral edema. *Neurol Sci* 32, 113-116.
- Igarashi, H., Tsujita, M., Suzuki, Y., Kwee, I.L., and Nakada, T. (2013). Inhibition of aquaporin-4 significantly increases regional cerebral blood flow. *Neuroreport* 24, 324-328.
- Jiang, R., Diaz-Castro, B., Looger, L.L., and Khakh, B.S. (2016). Dysfunctional Calcium and Glutamate Signaling in Striatal Astrocytes from Huntington's Disease Model Mice. *J Neurosci* 36, 3453-3470.
- Mayo, F., Gonzalez-Vinceiro, L., Hiraldo-Gonzalez, L., Calle-Castillejo, C., Morales-Alvarez, S., Ramirez-Lorca, R., and Echevarria, M. (2023). Aquaporin-4 Expression Switches from White to Gray Matter Regions during Postnatal Development of the Central Nervous System. *Int J Mol Sci* 24.
- Mola, M.G., Sparaneo, A., Gargano, C.D., Spray, D.C., Svelto, M., Frigeri, A., Scemes, E., and Nicchia, G.P. (2016). The speed of swelling kinetics modulates cell volume regulation and calcium signaling in astrocytes: A different point of view on the role of aquaporins. *Glia* 64, 139-154.

Risher, W.C., Andrew, R.D., and Kirov, S.A. (2009). Real-time passive volume responses of astrocytes to acute osmotic and ischemic stress in cortical slices and in vivo revealed by two-photon microscopy. *Glia* 57, 207-221.

Salman, M.M., Kitchen, P., Yool, A.J., and Bill, R.M. (2022). Recent breakthroughs and future directions in drugging aquaporins. *Trends Pharmacol Sci* 43, 30-42.

Shigetomi, E., Bushong, E.A., Hausteiner, M.D., Tong, X., Jackson-Weaver, O., Kracun, S., Xu, J., Sofroniew, M.V., Ellisman, M.H., and Khakh, B.S. (2013). Imaging calcium microdomains within entire astrocyte territories and endfeet with GCaMPs expressed using adeno-associated viruses. *J Gen Physiol* 141, 633-647.

Solenov, E., Watanabe, H., Manley, G.T., and Verkman, A.S. (2004). Sevenfold-reduced osmotic water permeability in primary astrocyte cultures from AQP-4-deficient mice, measured by a fluorescence quenching method. *Am J Physiol Cell Physiol* 286, C426-432.

Verkman, A.S., Binder, D.K., Bloch, O., Auguste, K., and Papadopoulos, M.C. (2006). Three distinct roles of aquaporin-4 in brain function revealed by knockout mice. *Biochim Biophys Acta* 1758, 10851093.

<https://doi.org/10.7554/eLife.95873.2.sa0>